

# Evolution in unrest processes at Campi Flegrei caldera as inferred from local seismicity

Stefania Danesi<sup>1</sup>, Nicola Alessandro Pino<sup>2</sup>, Stefano Carlino<sup>2</sup>, Christopher R.J. Kilburn<sup>3</sup>

<sup>1</sup>Istituto Nazionale di Geofisica e Vulcanologia, Sezione di Bologna, Bologna, IT

<sup>2</sup>Istituto Nazionale di Geofisica e Vulcanologia, Sezione di Napoli, Napoli, IT

<sup>3</sup>UCL Hazard Centre, Department of Earth Sciences, University College London, London, UK

Corresponding Authors

stefania.danesi@ingv.it

alessandro.pino@ingv.it

## Highlights

- Low permeability barriers modulate fluid circulation to favour seismicity
- The unrest of 1982-84 decelerated after a seismic swarm on April 1<sup>st</sup>, 1984
- The 2005-23 uplift is associated with higher (and increasing)  $b$ -value than in 1982-84
- The current uplift will likely proceed until fracturing allows fluid depressurization

## Abstract

Changes in seismicity with time and location are diagnostic signals for understanding the dynamics of volcanic unrest. We used these signals at the Campi Flegrei caldera, in southern Italy, to investigate how structural changes have determined three styles of unrest since 1982, distinguished by a ground uplift (measured at Pozzuoli, near the centre of the caldera) of 178 cm in 1982-84; a subsidence of 93 cm in 1985-2005; and an uplift of 118 cm between 2005 and November 2023. Double-difference seismic locations and concentrations of seismic energy release have revealed impermeable horizons that correspond to the cap rock and self-sealed base of the geothermal system at depths of 1.5 and 3 km, respectively. Most earthquakes have been shallower than 3 km, consistent with the

28 brittle upper crust being stretched over a zone of pressurization below the geothermal system. The  
129 1982-84 uplift decayed after a major seismic swarm on April 1<sup>st</sup>, 1984, breached the lower imper-  
2  
330 meable horizon, which increased the flux of escaping gas and reduced the source pressure. Contin-  
4  
5  
631 ued gas escape promoted subsidence until the lower horizon had resealed itself and initiated a new  
7  
832 episode of uplift while gas from depth re-accumulated beneath. Compared with 1982-84, a greater  
9  
10  
1133 proportion of recent seismicity has occurred at shallower depths below the actively degassing fuma-  
12  
1334 roles of Solfatara-Pisciarelli, north-east of Pozzuoli. The associated high seismic *b*- values, between  
14  
15  
1635 1 and 2, are consistent with high fluid pressures and, hence, with locations more favourable to frac-  
17  
1836 turing. Continued uplift may thus persist until fracturing of the shallow crust allows faster rates of  
19  
20  
2137 gas release and depressurization of the pressure source.

22  
2338

24  
25  
2639 **Keywords: (Max. 6)**

27  
28  
2940 Campi Flegrei caldera (CFc), Volcanic unrest, Hydrothermal system, Seismicity, Fluid circulation,  
30  
31  
3241 Brittle/ductile transition

33  
34  
3542

## 36 37 3843 **1. Introduction**

39  
4044 Campi Flegrei is the largest active caldera in Europe (~12 km diameter) with a population of more  
41  
4245 than 360,000 people. From the suburbs of Naples, it extends westward to the Tyrrhenian Sea and is  
43  
44  
4546 partially submerged below the Pozzuoli Bay (Fig 1A). Since pre-Roman times, the Campi Flegrei  
46  
4747 caldera (CFc) has shown a background trend of slow subsidence occurring at a rate of about 1-  
48  
49  
5048 2 cm/yr, interrupted by episodes of faster ground uplift (Dvorak and Mastrolorenzo, 1991; Bellucci  
51  
5249 et al., 2006; Di Vito et al., 2016; De Vivo et al., 2020) accompanied by widespread occurrences of  
53  
54  
5550 volcano-tectonic (VT) seismicity (Corrado et al., 1977; Del Pezzo et al., 1987; Petrosino et al.,  
56  
5751 2008). Since 1950 four episodes of caldera-wide ground deformation have raised the coastal town  
58  
5952 of Pozzuoli, located near the centre of largest uplift, by more than 4 m (Fig. 1B; Del Gaudio et al.,  
60  
61  
62  
63  
64  
65

53 2010). The first three episodes interrupted the secular subsidence of the caldera with comparable  
154 amounts of uplift in both duration and amplitude: about 74 cm in 1950-52, 159 cm in 1970-72, and  
2  
355 178 cm in 1982-84 (Fig. 1B; Del Gaudio et al., 2010). Scarce seismic activity was observed during  
4  
5  
656 the 1970-1972 unrest. In contrast, the seismic stations of the Osservatorio Vesuviano (OV) recorded  
7  
857 more than 16,000 shallow VT earthquakes (with maximum magnitude  $M_d=4.0$ ) during the 1982–84  
9  
10  
1158 crisis (OV; Del Pezzo et al., 1987; Petrosino et al., 2008), coinciding with an uplift at Pozzuoli of  
12  
1359 about 178 cm between June-July 1982 and the end of December 1984 (Dvorak and Berrino, 1991;  
14  
15  
1660 Del Gaudio et al., 2010; De Martino et al., 2021). Subsidence began shortly after and continued for  
17  
1861 c. 20 years, lowering Pozzuoli by 93 cm, at an average rate 2.6 times faster than secular subsidence.  
19  
20  
2162 Unrest returned in 2005 with the lowest rate of uplift in the last century (c. 5 cm/year; Figs 1B and  
22  
2363 1C). By April 2022, the uplift had recovered the previous two decades of subsidence (INGV, 2023).  
24  
2564 Persistent seismicity returned in 2012-14, since when the mean rate has continued to increase (Fig.  
26  
27  
2865 1C) and, by February 2023, more than 7000 events had been detected (INGV, 2023).  
29  
30  
3166 The VT events at CFc have occurred at depths of about 3 km or less, within crust that hosts a high-  
32  
3367 temperature hydrothermal system (temperature gradients in deep boreholes exceed 150 °C/km to  
34  
3568 depths of 3 km), the base of which appears to correspond to the brittle-ductile transition zone  
36  
37  
3869 (BDTZ) (Carlino, 2018; Castaldo et al., 2019). VT events can be triggered by several processes, in-  
39  
40  
4170 cluding changes in the stress field of the host rocks, directly induced by the uplift and migration of  
42  
4371 magma or magmatic fluids (Suzuki, 1959; White and McCausland, 2016); the tendency to increase  
44  
4572 fracture density in highly heterogeneous materials (Mogi, 1962); thermal stress, particularly in the  
46  
47  
4873 presence of hot fluids causing high thermal gradients (Warren and Latham, 1970). At the CFc, the  
49  
5074 VT seismicity and ground movement have been driven by changes in the volcanic-magmatic system,  
51  
52  
5375 rather than the regional stress across the caldera (Rivalta et al., 2019). Specific controls have been  
54  
5576 linked to spatial and temporal variations in the stress field associated with volcanic dynamics (Dvo-  
56  
57  
5877 rak and Berrino, 1991; Macedonio et al., 2014; D'Auria et al., 2015) or to fluid circulation within  
59  
6078 the hydrothermal system (Di Luccio et al., 2015; Chiodini et al., 2021; Petrosino and De Siena,  
61  
62  
63  
64  
65

79 2021). In addition to VT events, long-period (LP) earthquakes are rarely recorded in the CFc, main-  
180 ly due to perturbations in the shallow pressure field that induce resonance in fluid-generated frac-  
2 tures (Cusano et al., 2008).  
3  
4  
5  
6  
7  
8  
9  
10  
11  
12  
13  
14  
15  
16  
17  
18  
19  
20  
21  
22  
23  
24  
25  
26  
27  
28  
29  
30  
31  
32  
33  
34  
35  
36  
37  
38  
39  
40  
41  
42  
43  
44  
45  
46  
47  
48  
49  
50  
51  
52  
53  
54  
55  
56  
57  
58  
59  
60  
61  
62  
63  
64  
65

81 tures (Cusano et al., 2008).

82 The unrest episodes have been caused by pressure changes in fluids below the BDTZ at depths of c.

83 3-4 km (Dvorak and Berrino, 1991; Gottsmann et al., 2006a; Gottsmann et al., 2006b; Woo and

84 Kilburn, 2010; D’Auria et al., 2011; Troise et al., 2019) which, in turn, may have disrupted the cir-

85 culation of fluids within the overlying hydrothermal system and reinforced the total amount of sur-

86 face deformation and VT seismicity (Di Luccio et al., 2015; Tamburello et al., 2019; Chiodini et al.,

87 2021; Petrosino and De Siena, 2021; Lima et al., 2021; Todesco, 2021; Bonafede et al., 2022; Bu-

88 no et al., 2022).

89 The fluids available below the BDTZ are magma or magmatic gas, notably CO<sub>2</sub> (Buono et al., 2022).

90 The sources for both are a melt-rich zone about 7-9 km below the surface (Tamburello et al., 2019;

91 Chiodini et al., 2021; Buono et al., 2022).

92 The gas is dominated by CO<sub>2</sub> (Caliro et al., 2007; 2014; Chiodini et al., 2021) which, during the

93 first half of 2023, had an average flux of c. 4000 tonnes/day from the Solfatara-Pisciarelli fumaroles,

94 c. 2-2.5 km NE of Pozzuoli harbour (INGV, 2023). Although 20-40% may be non-magmatic

95 (caused by decarbonation of hydrothermal calcite; Buono et al. (2023)), the magmatic component

96 remains comparable to fluxes at active volcanoes with sustained outgassing (INGV, 2023).

97 The evolving behaviour during successive episodes of unrest (with variations in ground deformation,

98 seismicity rate and geochemical parameters) is consistent with a single, long-term sequence of crus-

99 tal extension (Kilburn et al., 2017; 2023). The dominant fluid being pressurized beneath the BDTZ

100 may also have changed between episodes from magma during the short, rapid uplifts before 1984 to

101 magmatic gas during the slow, long uplift since 2004 (Kilburn et al., 2023). Here, we compare the

102 patterns of VT seismicity during the current (since 2005) and previous (1982-84) episodes of unrest

103 to identify new constraints on structural changes in the crust and the evolution of the ongoing unrest.

104 Our results show that the caldera’s behaviour since 1982 is consistent with a single, long-term re-

105 sponse to pressurization in 1982-84 breaching impermeable horizons beneath the geothermal sys-  
106 tem and disrupting the flow of magmatic gas through the upper crust. They also suggest that contin-  
107 ued unrest will favour more extensive fracturing and gas release, with outcomes ranging from a de-  
108 celeration in ground movement to phreatic explosions and, in the extreme, to conditions suitable for  
109 renewed magma ascent from depth.

10  
11  
12

## 11 2. Data and Methods

112 To examine the seismic characteristics of CFC's unrest, we first derived the relative locations, rates  
113 of energy release and magnitude-frequency relations for earthquakes since 1982.

14  
15  
16  
17  
18  
19  
20  
21  
22

### 21 2.1 Double-difference earthquake location

215 The 1982-84 unrest was monitored by a local network of vertical-component, short-period, analog  
216 seismic stations (Fig. 1A), with estimated magnitude of completeness  $M_c=0.5$  (Scarpa et al., 2022).

217 It was supplemented between August 1983 and May 1984 by a temporary three-component, short-  
218 period, digital network from the University of Wisconsin (Aster and Meyer, 1988). Since the early  
219 2000s, the network has been significantly modernised and its performance has improved (Bianco et  
220 al., 2022). At the time of writing, the seismic network consists of 26 broad-band 3-component digi-  
221 tal stations, with real-time data transmission (Fig. 1A). The completeness magnitude for the net-  
222 work is 0.2 (Tramelli et al., 2021).

223 Seismicity was almost absent during the subsidence between 1985 and 2005; it occurred only in a  
224 very restricted area around Solfatara, in the form of short-lived swarms (one or a few days) spaced  
225 months or years apart. (Fig. 1C; Orsi et al., 1999; D'Auria et al., 2011; Global Volcanism Program,  
226 1989). For this reason we neglected the 1984-2004 interval, and focused instead on the seismicity of  
227 the unrest 1982-84 and 2005-23. Time series for the daily number of earthquakes show that swarm  
228 activity superimposed on more continuous seismic activity during both intervals (Fig. 1C;  
229 Supplementary Materials).

61  
62  
63  
64  
65

130 For the two time intervals 1982-84 and 2005-23, we analysed the differential P and S arrival times  
131 for pairs of events extracted from the manually revised INGV-Naples database to perform a relative  
132 double-difference location with the HypoDD algorithm (Waldhauser, 2001). Arrival times at sta-  
133 tions operating in both periods were included. We examined the two seismic datasets separately to  
134 account for disparities in the monitoring system, while maintaining the same inversion scheme. We  
135 first performed the absolute location for all events with the Hypoinverse algorithm (Klein, 2002)  
136 using station delay time when known, distance weighting for P and S arrival times, and an *ad-hoc*  
137 calibrated 1D reference seismic velocity model (Table 1S Supplementary Materials). Based on the  
138 differential travel times of the event pairs, the pre-processing of the double-difference inversion se-  
139 lected 8142 and 5037 linked events, respectively for the years 1982-84 and 2005-23 (Fig. 1D and  
140 Fig. 1E, green dots). The inversion procedure required: three sets of iterations; the use of the Least  
141 SQuaRe (LSQR) algorithm which is suitable for large datasets; at least 8 observations per pair of  
142 events; weighted P and S arrival times; a maximum distance of 2 km between linked events; and a  
143 damping parameter equal to 200.

## 144 **2.2 Seismic energy release**

145 We estimated the cumulative square root of the seismic energy release as a proxy for co-seismic  
146 strain release (Benioff, 1951). We used the duration magnitude  $M_d$ , which is the measure of earth-  
147 quake magnitude that INGV in Naples routinely estimates and officially communicates to the Na-  
148 tional Civil Protection in the INGV Seismic Bulletins (INGV, 2023). This measure is preferred to  
149 account for the large percentage of micro-seismicity ( $M_d < 1$ ) and to maintain homogeneity with cat-  
150 alogues from 1982 onward. It is manually calculated from the waveform coda at a short-period  
151 seismic station (STH, in Fig. 1A). We derived the moment magnitude ( $M_w$ ) from catalogues of  $M_d$   
152 for the two periods of unrest (Ricciolino and Lo Bascio 2021; Tramelli, 2022), by applying the em-  
153 pirical magnitude-duration relation of Orsi et al. (1999) and calibration laws for magnitude scales  
154 from Petrosino et al. (2008). To estimate the cumulative seismic energy distribution  $E_s$ , we divided

155 the seismogenic volume into a regular grid with nodes 0.2 km apart and applied the energy-  
156 magnitude relationship of Kanamori (1977):  $\log E_s = 11.8 + 1.5M_w$ .

## 157 **2.3 Gutenberg-Richter $b$ -value and stress patterns**

158 We calculated the seismic  $b$ -value (Gutenberg and Richter, 1955) to investigate variations in the  
159 size distribution of earthquakes and its relation to changes in local stress. For the size distribution,  
160 we used the relative earthquake locations on a regular grid with 0.05 km spacing. Each estimate was  
161 based on at least 150 events, of which at least 50 with duration magnitudes above the completeness  
162 value  $M_c$  within 0.5 km from each grid node;  $M_c$  was obtained by the maximum curvature tech-  
163 nique (Wiemer and Wyss, 2000). To investigate changes in local stress after seismic swarms, we  
164 calculated changes in  $b$ -value for VT events in a cylindrical volume centered on Solfatara and, with  
165 a radius of 0.7 km, large enough to include a representative proportion of swarms (Supplementary  
166 Materials, Table S2).

## 168 **3. Results**

### 169 **3.1 Relative locations of earthquakes**

170 As shown in Figs 1D and 1E, the HypoDD inversion returned the relative location for 3062 events  
171 in 1982-84 (time residuals of 0.05-0.4 s with a median of 0.9 s) and of 3355 events in 2005-23 (time  
172 residuals of 0.01-0.09 s with a median of 0.04 s). The median spatial errors for the three compo-  
173 nents are in the range 77-100 m for 1982-84 and 31-40 m for 2005-23.

### 174 **3.2 Evolution of seismicity patterns over time**

#### 175 *3.2.1 1982-1984*

176 Figures 2 and 3 show the time evolution of the 1982-84 seismicity projected over two sets of or-  
177 thogonal vertical sections with principal directions NW-SE along the caldera's coastline and N-S  
178 across Solfatara. Only sporadic and weak seismicity occurred until the first half of 1983, after

179 which the event rate accelerated significantly (Fig. 2A). The coastline section shows two broad  
180 clusters of events: one about 2 km wide at depths of 1.5-3 km below Pozzuoli (Fig. 2A), and another  
181 with an oblique, upward alignment between 3 and 0.5 km below Solfatara (Fig. 2A and 3A).  
182 Fewer events occurred offshore. In the southwestern part of the Bay of Pozzuoli, they showed a  
183 NW-SE alignment (Figs 2B) along a recognized fault structure (Di Luccio et al., 2015; Natale et al.,  
184 2022). The sub-horizontal cluster at depths of 1.0-1.5 km between Solfatara and Pozzuoli (Fig. 3A)  
185 represents the upper limit for seismicity west of Solfatara throughout the entire unrest. In the NS  
186 direction the seismicity did not extend more than 1 km from Solfatara, apart from a small cluster 1.5  
187 km deep on the edge of the Astroni crater and about 2 km north of Solfatara (Fig. 3).

188 On April 1<sup>st</sup>, 1984, a swarm of over 500 events (Barberi et al., 1984) occurred beneath Pozzuoli  
189 (Fig. 2A and Fig. 3B, dark red circles) at depths between 1 and 3 km; the two largest events with  
190  $M_d=3.0$  occurred at 04:27AM UTC and 04:43AM UTC (Tramelli, 2021).

191 For this swarm, we analysed data from 368 events in the  $0.2 \leq M_d \leq 3.0$  magnitude range and obtained  
192 217 relative HypoDD locations with a minimum  $M_d$  of 0.4 (Fig. 4). The epicentres closely followed  
193 the marine terrace of La Starza (Fig. 4A), while the hypocenters occurred along a well-defined  
194 oblique alignment between depths of 1 and 3 km. Larger events tended to occur at greater depths  
195 and all those with  $M_d \geq 2$  were deeper than 2 km (Fig. 4C). The distributions together indicate the  
196 activation of a c.  $2 \times 2$  km<sup>2</sup> structure dipping at high-angle towards the SW (Fig. 4B and 4C). The  
197 swarm marked a change in ground movement and the pattern of seismicity. First, the rate of ground  
198 uplift began a long-term decay from its peak value of c. 0.2 cm/day until the end of unrest (Fig. 4D).  
199 Second, although 1.5 km away from the swarm itself (Fig. 3B), Solfatara became a focus for large-  
200 magnitude events: before the swarm, only two events with magnitudes  $M_d \geq 3$  had occurred in its vi-  
201 cinity, on 24 November ( $M_d=3.5$ ) and 30 December 1983 ( $M_d=3.8$ ; Fig. 3A, green circle); after the  
202 swarm, in contrast, locations beneath Solfatara produced most of the high-magnitude events until  
203 the end of unrest (more than 30 with  $M_d \geq 3$ ; Fig. 3).

### 204 3.2.2 2005-2023



205 The 1984 crisis was followed by twenty years of occasional seismicity while the ground subsided  
206 by c. 0.9 m (Fig. 1C). Weak seismicity resumed c. 1 km NE of Solfatara when uplift began again in  
207 2004-2005. By February 2023, three spatially distinct clusters could be recognised from the WSW-  
208 ENE profile in Fig. 5A:

209 (i) An oblique alignment deepening from about 2 km beneath Solfatara to c. 3 km about 1.5 km to  
210 the northeast.

211 (ii) A sub-horizontal cluster at depths of 1.0-1.5 km in the hydrothermal system between Solfatara  
212 and Pozzuoli. It extends laterally for less than 1.5 km and, with the exception of a very shallow  
213 oblique alignment extending towards the coast line, marks the upper limit for seismicity west of  
214 Solfatara (Fig. 5A). The extent of this cluster confirms the presence of a fracture-resistant cap rock  
215 overtopping the seismogenic volume W of Solfatara, previously identified by Vanorio and Kanit-  
216 panyacharoen (2015) and imaged by velocity and attenuation tomography (Calò and Tramelli, 2018;  
217 De Siena et al., 2017)

218 (iii) Since 2018, a shallow cluster (at depths of less than 1 km) appears to have been developing  
219 beneath Solfatara in the direction of Pisciarelli to the northeast.

220 The perpendicular profile (Fig. 5B) highlights the migration of events shallower than 1.5 km to-  
221 wards the southeast, and the lack of significant seismicity more than 1 km from Solfatara and deep-  
222 er than 1-1.5 km.

### 223 **3.3 Comparative distributions of earthquakes in 1982-84 and 2005-23**

224 Low seismicity has occurred west of Solfatara in 2005-2023. At depths of 1.5-3.0 km between Poz-  
225 zuoli and Solfatara, only isolated and low-energy events have occurred since 2005, in contrast to the  
226 pronounced seismicity in 1982-84 that included duration magnitudes greater than 3. The difference  
227 has been accentuated by the cluster of events developing at depths of 2-3 km beneath Solfatara  
228 since 2005. This cluster appears to be slightly shifted to the NE compared with 1982-84. Another

229 new feature is the cluster of shallow earthquakes extending from depths of 0.5-1.km toward Pisci-  
230 arelli; seismicity in this volume was barely evident in 1982-84 (Figs 6A and 6B).

231 For both periods, low-magnitude seismicity has been distributed between Pozzuoli and Solfatara, at  
232 a depth of 1-1.5 km (B-C-D-E), with the density of events increasing towards Solfatara.

233 In 1982-84 a major offshore structure was active 2-3 km from the coast, oriented NW-SE and about  
234 3 km long. The orientation of the fault structure changes with depth. Thus its mean dip is c. 70° SW  
235 (Fig. 6A, Profiles A-C) between 2 and 4 km below the surface, but sub-vertical (possibly dipping  
236 steeply to the NE) at shallower levels (Fig. 6A, Profiles D-F). The angles are consistent with previ-  
237 ous estimates based on a smaller number of events (Orsi et al., 1999). All the events with  $M_d \geq 3$  oc-  
238 curred along the deeper segment (Figs 2B & 6A). After 2005, the segment between 2 and 3.5 km  
239 depth of the same structure was activated, with a significant event ( $M_d=3$ , reverse mechanism from  
240 INGV Bulletin data; INGV, 2023) on 2023/02/05.

### 241 **3.4 Energy Release**

242 The total Benioff strain released during the 1982-84 unrest is more than one order of magnitude  
243 larger than that released during 2005-23 (Fig. 7). For 1982-84, horizontal (Fig. 4Sb) and vertical  
244 sections (Fig. 7) indicate that most of the strain energy was concentrated along a horizontal belt that  
245 extended across the caldera, at a depth between 2 and 3 km. Peak values within this horizon were  
246 located beneath Solfatara. A smaller concentration can also be seen at depths of c. 1.5 km and be-  
247 low Solfatara (Fig. 7). At depths greater than 3 km, strain tends to have accumulated beneath the  
248 outer margins of ground uplift (Fig. 4Sb).

249 For 2005-23 the strain has instead been focused in small volumes corresponding to the three  
250 main clusters of earthquake locations (Section 3.2.2): along the 1-1.5 km horizon between Solfatara  
251 and Pozzuoli; about 0.5-1.0 km below Solfatara-Pisciarelli; and in a volume 1 km NE of Solfatara at  
252 depths of 2.5-3 km.

### 253 **3.5 Gutenberg-Richter $b$ -value**

254 The magnitude-frequency distribution of earthquakes in 1982-84 has a seismic  $b$ -value of  $0.89\pm 0.02$   
1  
255 (Fig. 8). Maximum values occurred among earthquakes below Solfatara (depths  $<1$  km) and the po-  
3  
4  
556 sition of maximum uplift near Pozzuoli (depth of c. 1-1.5 km and c. 2-3 km). In 2005-23, the  $b$ -  
6  
7  
857 value was  $0.92\pm 0.02$ , with peak values up to  $2\pm 0.03$ , again below Solfatara (depths  $<0.5$  km) and  
9  
10  
1158 close to the centre of uplift (depths c. 1.0-1.6 km); a small concentration is also apparent about 1.5  
12  
1359 km west of Solfatara at a depth of c. 1 km (Fig. 8). Peak values of the  $b$ -value for the current unrest  
14  
15  
1660 are generally higher than for the 1982-84 unrest.  
17  
18  
1961 Since 2020, the  $b$ -value has been increasing by about 70-80% beneath Solfatara and Pisciarelli to a  
20  
2162 depth of 2.5 km, as well as in the 1.5 km horizon west of Solfatara (Fig. 9). Increases in  $b$ -value be-  
22  
23  
2463 neath Solfatara are roughly related to the occurrence of swarms (Fig. 7S).  
25  
26  
2764  
28  
29

## 3065 4. Discussion

### 3166 4.1 Major patterns of seismicity

32  
33  
3467 Seismicity in 1982-84 and 2005-23 has been dominated by movements across related sets of faults.  
35  
36  
3768 In 1982-84, almost all earthquakes occurred at depths of less than 3.5-4 km and had epicentres dis-  
38  
39  
4069 tributed close to the coastline, starting east of Solfatara and crossing the hydrothermal system to the  
41  
4270 west (Fig. 6). For both periods, most of the largest events have been located at depths of 2-3 km,  
43  
44  
4571 near the base of a NE-dipping structure that defines the eastern boundary of the seismic zone (Fig.  
46  
4772 6). A secondary concentration of epicentres occurs along a NW-SE alignment 2.5 km to the south-  
48  
49  
5073 west, beneath the Bay of Pozzuoli (Fig. 6).  
51

5274 The limiting depth of c. 3 km for seismicity and strain energy release lies close to the depths of the  
53  
54  
5575 Brittle-Ductile Transition Zone (Carlino, 2018; Castaldo et al., 2019) and to the locations of pres-  
56  
57  
5876 sure sources inferred from patterns of ground deformation (Dvorak and Berrino, 1991; Gottsmann  
59  
6077 et al., 2006a; Gottsmann et al., 2006b; Woo and Kilburn, 2010; D'Auria et al., 2011; Troise et al.,  
61  
62  
63  
64  
65

278 2019). Apart from the shallow seismicity below Solfatara, few earthquakes have occurred at depths  
279 less than 1 km (Fig. 6). This depth approximately coincides with the base of a fracture-resistant cap  
280 rock proposed by Vanorio and Kanitpanyacharoen (2015). Such a horizon would promote fluid ac-  
281 cumulation in the underlying rock and the onset of fluid-induced fracturing (Akande et al., 2021).

282 The seismogenic zone of the CFc thus appears to be bounded (1) by two levels where the crust's  
283 mechanical properties change significantly (a strong, shallow cap rock and a deeper transition from  
284 a brittle to ductile rheology), and (2) by well-established fault systems around its lateral margins.

285 Despite these common features and the similarity in the quasi-radial symmetric pattern of ground  
286 deformation (Berrino et al., 1994; De Martino et al., 2021), suggesting a similar source location and  
287 overpressure value, the uplift rate (Fig. 1 C), the spatial distribution of seismicity (Fig. 6), and the  
288 seismic energy release (Fig. 7) show significant differences for the two periods 1982-84 and 2005-  
289 23. In particular, for the current unrest, the uplift rate is about 8 times lower than in 1982-84,  
290 earthquakes below the point of maximum uplift are substantially absent, while the seismically  
291 released energy is one order of magnitude lower than in 1982-84 and mainly located in narrow  
292 volumes below Solfatara-Pisciarelli area.

#### 293 **4.2 Structural changes in the crust since 1982-84.**

294 The base of the seismogenic zone corresponds with the BDTZ inferred from the temperatures and  
295 compositions of rocks from deep borehole (e.g. Carlino, 2018 and references therein). Adapting the  
296 model of Fournier (1999), we interpret this layer to be a self-sealing horizon that separates deeper  
297 crust that can achieve lithostatic pore pressure from overlying crust at hydrostatic pore pressure.

298 Lithostatic pore pressures below the BDTZ are favoured by CO<sub>2</sub> from depth maintaining a gas-  
299 saturated crust. We suggest that the sealed horizon was extended to breaking point during the 1982-  
300 84 crisis, caused by the intrusion of magma and its release of additional magmatic gas below the  
301 BDTZ. Before the seismic swarm of April 1<sup>st</sup>, 1984, by which time Pozzuoli had been raised by  
302 about 150 cm (Fig. 4D), the rate of uplift had been increasing (Fig. 4D) and most of the seismicity  
303 had occurred in a volume of c. 4-5 km<sup>3</sup> of the crust above the BDTZ (Figs 7 and 4Sa). After the

304 swarm, the rate of uplift began to decline (Fig. 4D), the number of earthquakes with magnitude  
305  $M_d \geq 3$  increased towards Solfatara (Figs 2 and 3) and the proportion of  $\text{CO}_2$  increased in the gases  
306 escaping from Solfatara (Chiodini et al., 2012). All three changes are consistent with the swarm  
307 breaching the BDTZ, allowing magmatic fluids and pressurised gases to escape into the overlying  
308 crust (Fig. 3S).

309 Magmatic gas that had accumulated in the pressure source escaped towards Solfatara, increasing the  
310 rate of  $\text{CO}_2$  emission and, by reducing the source pressure, initiated the decline in the rate of uplift  
311 (Fig. 4). The increase in the number of  $M_d \geq 3$  earthquakes would have also been favoured by a com-  
312 bination of perturbations in the shallow stress field at the time of the swarm and an increase in pore  
313 pressure from the gases migrating towards Solfatara. Depressurization due to a net loss in gas also  
314 explains the subsidence at the CFC between 1984 and 2004 (Todesco, 2021; Kilburn et al., 2023).

315 The seismically active segment above the BDTZ in 1982-84 has not shown the same diffuse seis-  
316 micity during the uplift since 2005, suggesting that some of the previous breaches were successfully  
317 resealed during the preceding subsidence. Resealing would also favour a return to slow uplift, when  
318 gases from magma 7-9 km underground were able to replenish the shallow source (Kilburn et al.,  
319 2023). Fig. 7 shows the thickness of the seismogenic crust using the depth of the 90% cut-off (D90)  
320 as a practical measure of the BDTZ (Supplementary Material). The shapes of the D90 levels in  
321 1982-84 and 2005-23 are remarkably similar and both become thicker away from the central area of  
322 the caldera between Pozzuoli and Solfatara (Fig. 7). However, the present depth of  $2.2 \pm 0.1$  km for  
323 the D90 boundary beneath Solfatara is less than its  $2.6 \pm 0.1$  km in 1982-84. The difference may re-  
324 flect local heating, and potential weakening, of the crust as a result of an increased supply of steam  
325 and magmatic gas (Chiodini et al., 2021), although, this remains a qualitative interpretation. In con-  
326 trast, the D90 boundary beneath Pozzuoli appears deeper today than it was in 1982-84. This sug-  
327 gests that it has not been similarly heated by gas flow, which is consistent with the BDTZ beneath  
328 Pozzuoli having become a sealed horizon.

### 329 **4.3 Focussed gas escape through Solfatara-Pisciarelli**

330 Resealing of the BDTZ across the central part of the caldera has focussed degassing beneath Solfa-  
331 tara. The concentration of low-magnitude seismicity below the eastern end of the cap rock (Figs 5  
2  
332 and 6) suggests that the accumulation of magmatic gas unable to escape through Solfatara has been  
4  
5  
333 a major control on the amount of local fracturing below Solfatara-Pisciarelli fumaroles. Seismicity  
7  
334 at the Solfatara end of the cap rock has also been characterised by *b*-values of between 1.4 and 2.0,  
9  
10  
1335 more than twice the background values of 0.8-0.9, both before breaching in 1982-84 and after re-  
12  
1336 sealing by 2005 (Fig. 8). High *b*-values, greater than those observed for purely tectonic event fre-  
14  
15  
1337 quency-magnitude distributions (Mogi, 1962; Warren and Latham, 1970), are promoted by local  
17  
1338 increases in pore pressure. Independent evidence for high local pore pressures is provided by seis-  
19  
20  
2339 mic tomography, which has recorded anomalously high values for seismic P-wave velocity, as well  
21  
22  
2340 as high values for the ratio of P- to S- wave velocities below Solfatara (Fig. 5S; Calò and Tramelli,  
24  
25  
2341 2018). The *b*-value below Solfatara-Pisciarelli has been gradually increasing since 2021 by about  
26  
27  
2342 70-80% (Fig. 9). By extension of our arguments for Solfatara, we attribute the increase to the accu-  
29  
30  
3343 mulation of magmatic gas beneath the whole of the deforming crust. Analogy with *b*-value data  
31  
32  
3344 from compressional failure (Scholz, 2015) may also indicate a decrease in the applied differential  
34  
3345 stress.

#### 3346 **4.4 Future scenarios**

3347 In addition to the increasing rates of low-magnitude seismicity, 14 earthquakes with magnitudes  $M_d$   
42  
3348 of 3 or more have occurred since 2019 - all at depths between 2 and 3.5 km and with epicentres  
43  
44  
4349 about 2.0-2.5 km away from the centre of uplift (beyond Solfatara and Pisciarelli to the NE and  
45  
46  
4350 along an offshore fault to the SW; Fig. 6). They are the first earthquakes of such magnitude to have  
47  
48  
49  
50  
5351 been recorded during the post-2005 uplift. Their late onset (compared to the beginning of unrest)  
52  
53  
5352 and hypocentral positions suggest that the slip along larger faults has been caused by the bending of  
54  
55  
5353 the crust exceeding a critical amount. One exception to the distribution is the magnitude 3.6 earth-  
56  
57  
5354 quake that occurred on 11 June 2023 along the western edge of La Starza at a depth of 2.7 km. The  
58  
59  
60  
6355 location lies at the western edge of the 1982-84 seismogenic zone and close to the BDTZ.  
61  
62  
63  
64  
65

356 The pressure source driving unrest at CFC lies beneath the geothermal system. Its location suggests  
357 that the BDTZ is strong, as well as impermeable, and acts as a natural barrier to the ascent of fluids,  
2  
358 whether magma or magmatic gas. Rupture and resealing of the BDTZ have thus modulated ground  
4  
5  
359 movement and seismicity by controlling the flow of magmatic fluids from below the geothermal  
7  
8  
360 system (Fig. 10). Uplift since 2005 has again extended the crust, bringing the BDTZ closer to con-  
9  
10  
11  
361 ditions favourable to renewed rupture and enhanced surface degassing (Kilburn et al., 2023). Poten-  
12  
13  
362 tial outcomes depend on where rupture occurs and how abruptly it changes the flow of gas. Assum-  
14  
15  
363 ing a pattern of rupture similar to that in 1984, scenarios range from a slowing of uplift, either to  
16  
17  
364 rest or to a renewed subsidence, to a geothermal explosion of gas and vaporised groundwater in the  
19  
20  
365 vicinity of Solfatara-Pisciarelli. However, the emergence of seismicity near the BDTZ away from  
21  
22  
366 Solfatara (Fig. 8) raises the possibility of enhanced gas release from parts of the caldera not affected  
24  
25  
367 by such surface activity during recent episodes of unrest.

27  
28  
368 An implicit assumption in these scenarios is that conditions have not changed significantly for re-  
29  
30  
369 leasing gas from the parent magmatic system 7-9 km below the surface. In this case, changes in gas  
32  
33  
370 flux can be related to changes in fluid pressure between the deep source (assumed constant) and the  
34  
35  
371 BDTZ (which changes with the rate of gas escape to the surface; Kilburn et al., 2023). An alterna-  
36  
37  
372 tive to be tested is that new magma arriving from depths greater than 9 km has pressurized the par-  
39  
40  
373 ent system, increasing its rate of gas release and so favouring both a faster rate of accumulation at  
41  
42  
374 the level of the BDTZ and continued surface uplift. In this case, the change in gas flux may reflect  
44  
45  
375 the approach to conditions suitable for renewed magma ascent and either a shallow intrusion and  
46  
47  
376 episode of rapid uplift, as in 1982-84 or, if the magma reaches the new rupture, a magmatic eruption.

49  
50  
377

## 5378 5. Conclusions

55  
5379 Since 1982, seismicity and strain energy release at Campi Flegrei have been concentrated between  
57  
58  
5380 two low-permeability horizons at depths of about 1.5 and 3 km, respectively. The horizons are natu-  
59  
60  
5381 ral controls on the circulation of fluids within the volcano's geothermal system. The deeper horizon  
62  
63  
64  
65

382 coincides with a Brittle-Ductile Transition Zone (BDTZ) along the base of the system: above the  
383 base, pore pressures are hydrostatic and the crust behaves in an elastic-brittle manner; below the  
384 base, pore pressures can reach lithostatic values and deformation is mostly aseismic. The shallower  
385 low-permeability horizon marks a cap rock that separates the circulation of near-surface fluids from  
386 the flow of fluids within the deeper levels of the geothermal system.

387 Ground movements have been controlled by pressure changes below the BDTZ. Uplift occurs when  
388 new fluids enter the crust that is already rich in CO<sub>2</sub>. The new fluids may be magma, gas released  
389 from that magma, or an increased discharge of gas from depth. They stretch the overlying crust until  
390 the BDTZ is ruptured. In 1982-84, the rapid uplift starting in June-July 1982 began to decay after  
391 the seismic swarm of April 1<sup>st</sup>, 1984. Nine months later, ground uplift had halted, to be followed by  
392 slow subsidence until 2004-05 and then the slow uplift that is still continuing (November 2023).

393 The sequence is consistent with rapid uplift during the intrusion of magma and release of its gas.  
394 The seismic swarm in April 1984 ruptured the BDTZ and allowed gas to escape. The rate of degas-  
395 sing increased from Solfatara-Pisciarelli and reduced pressure in the source region. Continued gas  
396 escape promoted subsidence until the BDTZ had resealed itself sufficiently to again trap gas arriv-  
397 ing from depth and to initiate slow uplift at a rate comparable to (but in the opposite direction of)  
398 that during the preceding uplift (Fig. 10). Resealing has also focused gas flow towards Solfatara-  
399 Pisciarelli, raising local pore pressures and thermal gradient and favouring the concentration of  
400 seismicity in the adjacent eastern section of the Starza fault (Figs 7 and 8).

401 Should the ongoing uplift continue (November 2023), a new episode of rupturing can be expected  
402 across the BDTZ. Potential outcomes range from a reversal of ground movement, in the least dan-  
403 gerous scenario, to geothermal explosions or possibly even a magmatic eruption, in the most cata-  
404 strophic scenario, if new magma were to reach the uppermost layers of the crust. Our results thus  
405 provide a foundation for integrating additional geophysical and geochemical monitoring data, as  
406 well as surface observations, to identify the likelihood of each scenario and when it might occur.

407



408 **Conflict of Interest**

409 The authors declare that the research was conducted in the absence of any commercial or financial  
2  
410 relationships that could be construed as a potential conflict of interest.  
4  
5  
6

411 **Funding**

412 SD, NAP and SC were funded by the BEST CaFE Project, under the INGV Working Earth Project,  
10  
11  
413 supported by the Ministry of University and Research.  
12  
13  
14

414 **Acknowledgments**

415 We are grateful to two anonymous reviewers for their constructive comments and valuable sugges-  
18  
19  
416 tions, which have greatly improved the quality of the manuscript. We thank Patrizia Ricciolino  
20  
21  
417 (“Laboratorio di Sismologia” INGV Naples) for providing us with the arrival times of the seismic  
22  
23  
418 phases. Maps and vertical sections are created using the Free and Open Source QGIS (2022) and  
24  
25  
419 GMT6 (Wessel et al., 2019). Some plots and data analysis are made with Rstudio (2022).  
26  
28  
29

3420 **Data Availability**

3421 Seismic data are available from the INGV-Naples Web Site ([www.ov.ingv.it](http://www.ov.ingv.it))  
34  
35

3422 **Credit authorship contribution statement**

3423 SD: Conceptualisation, Data analysis, Visualisation, Interpretation, Writing;  
40  
41  
424 NAP: Project PI, Conceptualisation, Methodology, Interpretation, Writing;  
42  
43  
4425 SC: Interpretation, Writing; CRJK: Interpretation, Writing.  
45  
46  
47

426

427

49

5428

52

53

54

53

56

430

57

58

531

60

432

62

63

64

65

**References**

1. Akande, W.G., Gan, Q., Cornwell, D.G., Siena, L.D., 2021. Thermo-Hydro-Mechanical Model and Cap rock Deformation Explain the Onset of an Ongoing Seismo-Volcanic Unrest. *J Geophys Res Solid Earth* 126. <https://doi.org/10.1029/2020jb020449>

- 433 2. Aster R.C., Meyer R.P., 1988. Three-dimensional velocity structure and hypocenter distribution  
434 in the Campi Flegrei caldera, Italy. *Tectonoph.* 149 (3-4), 195-218. [https://doi.org/10.1016/0040-  
3 1951\(88\)90173-4](https://doi.org/10.1016/0040-<br/>2 1951(88)90173-4)  
4
- 5  
436 3. Barberi, F., Corrado, G., Innocenti, F., Luongo, G., 1984. Phlegraean Fields 1982–1984: Brief  
7 chronicle of a volcano emergency in a densely populated area. *Bull. Volcanol.* 47, 175–185.  
8  
9  
10  
11 438 <https://doi.org/10.1007/bf01961547>  
12
- 13 439 4. Bellucci, F., Woo, J., Kilburn, C.R.J., Rolandi, G., 2006. Ground deformation at Campi Flegrei,  
14 Italy: implications for hazard assessment. *Geological Soc Lond Special Publ* 269, 141–157.  
15  
16 440 <https://doi.org/10.1144/gsl.sp.2006.269.01.09>  
17
- 18  
19  
20 442 5. Benioff, H., 1951. Earthquakes and rock creep. *BSSA*, 31–62.  
21
- 22  
23 443 6. Berrino, G., 1994. Gravity changes induced by height-mass variations at the Campi Flegrei cal-  
24 dera. *J Volcanol Geoth Res* 61, 293–309. [https://doi.org/10.1016/0377-0273\(94\)90010-8](https://doi.org/10.1016/0377-0273(94)90010-8)  
25  
26 444
- 27  
28 445 7. Bianco, F., Caliro, S., Martino, P. D., Orazi, M., Ricco, C., Vilardo, G., et al. 2022. Campi  
29 Flegrei, A Restless Caldera in a Densely Populated Area. *Active Volcanoes World*, 219–237.  
30  
31 446 [https://doi.org/10.1007/978-3-642-37060-1\\_8](https://doi.org/10.1007/978-3-642-37060-1_8)  
32  
33 447
- 34  
35 448 8. Bonafede, M., Amoroso, A., Crescentini, L., Gottsmann, J.H., Todesco, M., Trasatti, E., 2022.  
36 Campi Flegrei, A Restless Caldera in a Densely Populated Area. *Active Volcanoes World* 283–  
37  
38 449 309. [https://doi.org/10.1007/978-3-642-37060-1\\_11](https://doi.org/10.1007/978-3-642-37060-1_11)  
39  
40 450
- 41  
42  
43 451 9. Buono, G., Paonita, A., Pappalardo, L., Caliro, S., Tramelli, A., Chiodini, G., 2022. New Insights  
44 Into the Recent Magma Dynamics Under Campi Flegrei Caldera (Italy) From Petrological and  
45  
46 452 Geochemical Evidence. *J Geophys Res Solid Earth* 127. <https://doi.org/10.1029/2021jb023773>  
47  
48 453
- 49  
50 454 10. Buono, G., Caliro, S., Paonita, A., Pappalardo, L., Chiodini, G., 2023. Discriminating carbon di-  
51 oxide sources during volcanic unrest: The case of Campi Flegrei caldera (Italy). *Geology*.  
52  
53 455 <https://doi.org/10.1130/g50624.1>  
54  
55 456

- 457 11. Caliro, S., Chiodini, G., Moretti, R., Avino, R., Granieri, D., Russo, M., Fiebig, J., 2007. The  
458 origin of the fumaroles of La Solfatara (Campi Flegrei, South Italy). *Geochim. Cosmochim. Acta*  
2  
3459 71, 3040–3055. <https://doi.org/10.1016/j.gca.2007.04.007>  
4  
5  
460 12. Caliro, S., Chiodini, G., Paonita, A., 2014. Geochemical evidences of magma dynamics at Campi  
7  
8461 Flegrei (Italy). *Geochim. Cosmochim. Acta* 132, 1–15. <https://doi.org/10.1016/j.gca.2014.01.021>  
9  
10  
11462 13. Calò, M., Tramelli, A., 2018. Anatomy of the Campi Flegrei caldera using Enhanced Seismic  
12  
13463 Tomography Models. *Sci Rep-uk* 8, 16254. <https://doi.org/10.1038/s41598-018-34456-x>  
14  
15  
16464 14. Carlino, S., 2018. Heat flow and geothermal gradients of the Campania region (Southern Italy)  
17  
18465 and their relationship to volcanism and tectonics. *J Volcanol Geoth Res* 365, 23–37.  
19  
20466 <https://doi.org/10.1016/j.jvolgeores.2018.10.015>  
21  
22  
23467 15. Castaldo, R., D'Auria, L., Pepe, S., Solaro, G., Novellis, V.D., Tizzani, P., 2019. The impact of  
24  
25  
26468 crustal rheology on natural seismicity: Campi Flegrei caldera case study. *Geosci Front* 10, 453–  
27  
28  
29469 466. <https://doi.org/10.1016/j.gsf.2018.02.003>  
30  
31  
32470 16. Chiodini, G., Caliro, S., De Martino, P., Avino, R., Gherardi, F., 2012. Early signals of new vol-  
33  
34471 canic unrest at Campi Flegrei caldera? Insights from geochemical data and physical simulations.  
35  
36472 *Geology* 40, 943–946. <https://doi.org/10.1130/g33251.1>  
37  
38  
39473 17. Chiodini, G., Caliro, S., Avino, R., Bini, G., Giudicepietro, F., Cesare, W.D., Ricciolino, P.,  
40  
41474 Aiuppa, A., Cardellini, C., Petrillo, Z., Selva, J., Siniscalchi, A., Tripaldi, S., 2021. Hydrothermal  
42  
43475 pressure-temperature control on CO<sub>2</sub> emissions and seismicity at Campi Flegrei (Italy). *J*  
44  
45  
46476 *Volcanol Geoth Res* 107245. <https://doi.org/10.1016/j.jvolgeores.2021.107245>  
47  
48  
49477 18. Corrado, G., Guerra, I., Bascio, A.L., Luongo, G., Rampoldi, R., 1977. Inflation and microearth-  
50  
51478 quake activity of phlegraean fields, Italy. *Bull. Volcanol.* 40, 169–188.  
52  
53  
54479 <https://doi.org/10.1007/bf02596998>  
55  
56  
57480 19. Cusano, P., Petrosino, S., Saccorotti, G., 2008. Hydrothermal origin for sustained Long-Period  
58  
59481 (LP) activity at Campi Flegrei Volcanic Complex, Italy. *J. Volcanol. Geotherm. Res.* 177, 1035–  
60  
61482 1044. <https://doi.org/10.1016/j.jvolgeores.2008.07.019>  
62  
63  
64  
65

- 483 20.D’Auria, L., Giudicepietro, F., Aquino, I., Borriello, G., Gaudio, C.D., Bascio, D.L., Martini, M.,  
1  
284 Ricciardi, G.P., Ricciolino, P., Ricco, C., 2011. Repeated fluid-transfer episodes as a mechanism  
3  
4  
485 for the recent dynamics of Campi Flegrei caldera (1989–2010). *J Geophys Res Solid Earth* 1978  
6  
486 2012 116. <https://doi.org/10.1029/2010jb007837>  
8  
9  
1487 21.D’Auria, L., Pepe, S., Castaldo, R., Giudicepietro, F., Macedonio, G., Ricciolino, P., Tizzani, P.,  
11  
12  
1488 Casu, F., Lanari, R., Manzo, M., Martini, M., Sansosti, E., Zinno, I., 2015. Magma injection  
14  
15  
1489 beneath the urban area of Naples: a new mechanism for the 2012–2013 volcanic unrest at Campi  
17  
1490 Flegrei caldera. *Sci. Rep.* 5, 13100. <https://doi.org/10.1038/srep13100>  
19  
20  
2491 22.De Martino, P., Dolce, M., Brandi, G., Scarpato, G., Tammaro, U., 2021. The Ground Defor-  
22  
2492 mation History of the Neapolitan Volcanic Area (Campi Flegrei Caldera, Somma–Vesuvius Vol-  
24  
25  
2493 cano, and Ischia Island) from 20 Years of Continuous GPS Observations (2000–2019). *Remote*  
26  
27  
2494 *Sens-basel* 13, 2725. <https://doi.org/10.3390/rs13142725>  
29  
30  
3495 23.De Siena, L., Amoruso, A., Pezzo, E.D., Wakeford, Z., Castellano, M., Crescentini, L., 2017.  
32  
3496 Space-weighted seismic attenuation mapping of the aseismic source of Campi Flegrei 1983–1984  
34  
35  
3497 unrest. *Geophys Res Lett* 44, 1740–1748. <https://doi.org/10.1002/2017gl072507>  
37  
3498 24.De Vivo, B., Rolandi, G., 2020. Volcanological risk associated with Vesuvius and Campi Flegrei.  
39  
40  
499 Chapter in *Vesuvius, Campi Flegrei, and Campanian Volcanism*, 471-493.  
41  
42  
4500 <https://doi.org/10.1016/B978-0-12-816454-9.00017-1>  
44  
45  
4501 25.Del Gaudio, C., Aquino, I., Ricciardi, G.P., Ricco, C., Scandone, R., 2010. Unrest episodes at  
46  
47  
4502 Campi Flegrei: A reconstruction of vertical ground movements during 1905–2009. *J Volcanol*  
49  
50  
4503 *Geoth Res* 195, 48–56. <https://doi.org/10.1016/j.jvolgeores.2010.05.014>  
51  
52  
4504 26.Del Pezzo, E., De Natale, G., Martini, M., Zollo, A. 1987. Source parameters of microearth-  
53  
54  
4505 quakes at Phlegraean Fields (Southern Italy) volcanic area. *Phys Earth Planet In* 47, 25–42.  
56  
57  
4506 [https://doi.org/10.1016/0031-9201\(87\)90064-1](https://doi.org/10.1016/0031-9201(87)90064-1)  
58  
59  
60  
61  
62  
63  
64  
65

- 507 27.Di Luccio F, Pino N.A., Piscini A., Ventura G., 2015, Significance of the 1982–2014 Campi Fle-  
508 grei seismicity: Preexisting structures, hydrothermal processes, and hazard assessment. *Geophys.*  
2  
509 *Res. Lett.*, 42, 7498–7506. <https://doi.org/10.1002/2015GL064962>.  
4  
5  
510 28.Di Vito, M.A., Acocella, V., Aiello, G., Barra, D., Battaglia, M., Carandente, A., Del Gaudio, C.,  
7  
511 Vita, S. de, Ricciardi, G.P., Ricco, C., Scandone, R., Terrasi, F., 2016. Magma transfer at Campi  
9  
512 Flegrei caldera (Italy) before the 1538 AD eruption. *Sci Rep-uk* 6, 32245.  
10  
11  
513 <https://doi.org/10.1038/srep32245>  
12  
13  
14  
514 29.Dvorak, J.J., Berrino, G., 1991. Recent ground movement and seismic activity in Campi Flegrei,  
15  
16 southern Italy: Episodic growth of a resurgent dome. *J Geophys Res Solid Earth* 96, 2309–2323.  
17  
18  
515 <https://doi.org/10.1029/90jb02225>  
19  
20  
21  
22  
517 30.Dvorak, J. J., Mastrolorenzo, G., 1991.The mechanisms of recent vertical crustal movements in  
24  
25  
518 Campi Flegrei caldera, southern Italy. *Geological Society of America*  
26  
27  
519 <https://doi.org/10.1130/SPE263>, Springer ISBN 3540426426, 9783540426424  
29  
30  
31  
520 31.Fournier, 1999. Hydrothermal processes related to movement of fluid from plastic into brittle  
32  
33  
521 rock in the magmatic-epithermal environment. *Economic geology and the bulletin of the Society*  
34  
35  
522 *of Economic Geologists, Hydrothermal processes related to movement of fluid from plastic into*  
36  
37  
523 *brittle rock in the magmatic-epithermal environment* 94, 1193–1212.  
38  
39  
40  
524 32.Global Volcanism Program, 1989. Report on Campi Flegrei (Italy) (McClelland, L.,  
41  
42  
525 ed.). *Scientific Event Alert Network Bulletin*, 14:6. Smithsonian Institution.  
43  
44  
526 <https://doi.org/10.5479/si.GVP.SEAN198906-211010> (accessed October 2023)  
46  
47  
527 33.Gottsmann, J., Rymer, H., Berrino, G., 2006a. Unrest at the Campi Flegrei caldera (Italy): A crit-  
48  
49  
528 ical evaluation of source parameters from geodetic data inversion. *J Volcanol Geoth Res* 150,  
50  
51  
529 132–145. <https://doi.org/10.1016/j.jvolgeores.2005.07.002>  
53  
54  
530 34.Gottsmann, J., Folch, A., & Rymer, H., 2006b. Unrest at Campi Flegrei: A contribution to the  
56  
531 magmatic versus hydrothermal debate from inverse and finite element modeling. *Journal of Geo-*  
58  
59  
532 *physical Research: Solid Earth*, 111(B7). <https://doi.org/10.1029/2005JB003745>  
60  
61  
62  
63  
64  
65

- 533 35. Gutenberg, B., Richter, C.F., 1955. Magnitude and Energy of Earthquakes. *Nature* 176, 795–795.  
534 <https://doi.org/10.1038/176795a0>  
2
- 535 36. INGV 2023, Surveillance Bulletins <https://www.ov.ingv.it/index.php/monitoraggio-e->  
4  
5  
536 [infrastrutture/bollettini-tutti/bollett-mensili-cf/anno-2023-1](https://www.ov.ingv.it/index.php/monitoraggio-e-infrastrutture/bollettini-tutti/bollett-mensili-cf/anno-2023-1), in Italian  
7
- 537 37. Kanamori, H., 1977. The energy release in great earthquakes. *J Geophys Res* 82, 2981–2987.  
9  
538 <https://doi.org/10.1029/jb082i020p02981>  
10  
11
- 539 38. Kilburn, C.R.J., Natale, G.D., Carlino, S., 2017. Progressive approach to eruption at Campi Fle-  
14  
15  
540 grei caldera in southern Italy. *Nat Commun* 8, 15312. <https://doi.org/10.1038/ncomms15312>  
16  
17
- 541 39. Kilburn, C.R.J., Carlino, S., Danesi, S., Pino, N.A., 2023. Potential for rupture before eruption at  
19  
542 Campi Flegrei caldera, Southern Italy. *Commun. Earth Environ.* 4, 190.  
20  
21  
543 <https://doi.org/10.1038/s43247-023-00842-1>  
22  
23  
24
- 544 40. Klein, F.W., 2002. User’s guide to HYPOINVERSE-2000, a Fortran program to solve for earth-  
26  
27  
545 quake locations and magnitudes, Open-File Report 2002-171, <https://doi.org/10.3133/ofr02171>  
28  
29
- 546 41. Lima, A., Bodnar, R.J., Vivo, B.D., Spera, F.J., Belkin, H.E., 2021. Interpretation of Recent Un-  
31  
32  
547 rest Events (Bradyseism) at Campi Flegrei, Napoli (Italy): Comparison of Models Based on Cy-  
34  
548 clical Hydrothermal Events versus Shallow Magmatic Intrusive Events. *Geofluids* 2021, 1–16.  
36  
37  
549 <https://doi.org/10.1155/2021/2000255>  
38  
39
- 550 42. Macedonio, G., Giudicepietro, F., D’Auria, L., Martini, M., 2014. Sill intrusion as a source  
41  
42  
551 mechanism of unrest at volcanic calderas. *J. Geophys. Res.: Solid Earth* 119, 3986–4000.  
43  
44  
552 <https://doi.org/10.1002/2013jb010868>  
46
- 553 43. Mogi, K., 1962. Study of elastic shocks caused by the fracture of heterogeneous materials and its  
48  
49  
554 relations to earthquake phenomena. *Bull Earthquake Res Inst. Tokyo Univ.* 40(125), 196  
51
- 555 44. Natale, J., Camanni, G., Ferranti, L., Isaia, R., Sacchi, M., Spiess, V., Steinmann, L., Vitale, S.,  
53  
54  
556 2022. Fault systems in the offshore sector of the Campi Flegrei caldera (southern Italy): Implica-  
56  
557 tions for nested caldera structure, resurgent dome, and volcano-tectonic evolution. *J Struct Geol*  
58  
558 163, 104723. <https://doi.org/10.1016/j.jsg.2022.104723>  
59  
60  
61  
62  
63  
64  
65

- 559 45.Orsi, G., Civetta, L., Gaudio, C.D., Vita, S. de, Vito, M.A.D., Isaia, R., Petrazzuoli, S.M., Ric-  
560 ciardi, G.P., Ricco, C., 1999. Short-term ground deformations and seismicity in the resurgent  
2  
361 Campi Flegrei caldera (Italy): an example of active block-resurgence in a densely populated area.  
4  
562 J Volcanol Geoth Res 91, 415–451. [https://doi.org/10.1016/s0377-0273\(99\)00050-5](https://doi.org/10.1016/s0377-0273(99)00050-5)  
7
- 863 46.Petrosino, S., Siena, L.D., Pezzo, E.D., 2008. Recalibration of the Magnitude Scales at Campi  
9  
1064 Flegrei, Italy, on the Basis of Measured Path and Site and Transfer FunctionsRecalibration of the  
12  
1365 Magnitude Scales at Campi Flegrei, Italy. B Seismol Soc Am 98, 1964–1974.  
14  
1566 <https://doi.org/10.1785/0120070131>  
17
- 1867 47.Petrosino, S., Siena, L.D., 2021. Fluid migrations and volcanic earthquakes from depolarized  
19  
2068 ambient noise. Nat Commun 12, 6656. <https://doi.org/10.1038/s41467-021-26954-w>  
21  
22
- 2369 48.Polcari, M., Borgstrom, S., Gaudio, C.D., De Martino, P., Ricco, C., Siniscalchi, V., Trasatti, E.,  
24  
2570 2022. Thirty years of volcano geodesy from space at Campi Flegrei caldera (Italy). Sci Data 9,  
26  
2771 728. <https://doi.org/10.1038/s41597-022-01849-7>  
29
- 3072 49.QGIS Development Team, 2022. QGIS Geographic Information System. Open Source Geospa-  
31  
3273 tial Foundation Project. <http://qgis.osgeo.org>  
34
- 3574 50.Ricciolino, P., Lo Bascio, D., 2021. Cataloghi sismici dei vulcani campani. Stazione STH Campi  
36  
3775 Flegrei dal 2000 al 2021 (CatSTH\_2000\_2021) (1.0) [Data set]. Istituto Nazionale di Geofisica e  
38  
3976 Vulcanologia (INGV). [https://doi.org/10.13127/ovcatalogsth\\_2000\\_2021](https://doi.org/10.13127/ovcatalogsth_2000_2021)  
41
- 4277 51.Rivalta, E., Corbi, F., Passarelli, L., Acocella, V., Davis, T., Vito, M.A.D., 2019. Stress  
43  
4478 inversions to forecast magma pathways and eruptive vent location. Sci. Adv. 5, eaau9784.  
46  
4779 <https://doi.org/10.1126/sciadv.aau9784>  
48
- 4980 52.RStudio Team, 2022. RStudio: Integrated Development for R. RStudio, PBC, Boston, MA  
51  
5281 URL <http://www.rstudio.com/>.  
53  
54
- 5582 53.Scarpa, R., Bianco, F., Capuano, P., Castellano, M., D’Auria. L., Di Lieto, B., Romano., P., 2022.  
56  
57  
5883 Historic Unrest of the Campi Flegrei Caldera, Italy. In: Campi Flegrei, A Restless Caldera in a  
59  
6084 Densely Populated Area. Active Volcanoes World. <https://doi.org/10.1007/978-3-642-37060-1>  
62  
63  
64  
65

- 585 54.Scholz, C.H., 2015. On the stress dependence of the earthquake b value. *Geophys Res Lett* 42,  
586 1399–1402. <https://doi.org/10.1002/2014gl062863>
- 587 55.Siniscalchi, A., Tripaldi, S., Romano, G., Chiodini, G., Improta, L., Petrillo, Z., D'Auria, L.,  
588 Caliro, S., Avino, R., 2019. Reservoir Structure and Hydraulic Properties of the Campi Flegrei  
589 Geothermal System Inferred by Audiomagnetotelluric, Geochemical, and Seismicity Study. *J*  
590 *Geophys Res Solid Earth* 124, 5336–5356. <https://doi.org/10.1029/2018jb016514>
- 591 56.Suzuki, Z., 1959. A statistical study on the occurrence of small earthquakes (fourth paper). *Sci*  
592 *Rep Tohoku Univ Ser. 5, Geophysics* 11(1), 10–54
- 593 57.Tamburello, G., Caliro, S., Chiodini, G., De Martino, P., Avino, R., Minopoli, C., Carandente, A.,  
594 Rouwet, D., Aiuppa, A., Costa, A., Bitetto, M., Giudice, G., Francofonte, V., Ricci, T., Sciarra,  
595 A., Bagnato, E., Capecchiacci, F., 2019. Escalating CO<sub>2</sub> degassing at the Pisciarelli fumarolic  
596 system, and implications for the ongoing Campi Flegrei unrest. *J Volcanol Geoth Res* 384, 151–  
597 157. <https://doi.org/10.1016/j.jvolgeores.2019.07.005>.
- 598 58.Todesco, M., 2021. Caldera's Breathing: Poroelastic Ground Deformation at Campi Flegrei (Ita-  
599 ly). *Frontiers Earth Sci* 9, 702665. <https://doi.org/10.3389/feart.2021.702665>
- 600 59.Tramelli, A., Godano, C., Ricciolino, P., Giudicepietro, F., Caliro, S., Orazi, M., et al. 2021.  
601 Statistics of seismicity to investigate the Campi Flegrei caldera unrest. *Sci Rep-uk* 11, 7211.  
602 <https://doi.org/10.1038/s41598-021-86506-6>
- 603 60.Tramelli, A. 2022. Seismic catalogue Campi Flegrei 1982-1984 [Data set]. Zenodo.  
604 <https://doi.org/10.5281/zenodo.6810718>
- 605 61.Troise, C., De Natale, G., Schiavone, R., Somma, R., Moretti, R., 2019. The Campi Flegrei cal-  
606 dera unrest: Discriminating magma intrusions from hydrothermal effects and implications for  
607 possible evolution. *Earth-sci Rev* 188, 108–122. <https://doi.org/10.1016/j.earscirev.2018.11.007>
- 608 62.Vanorio, T., Virieux, J., Capuano, P., Russo, G., 2005. Three-dimensional seismic tomography  
609 from P wave and S wave microearthquake travel times and rock physics characterization of the



- 610 Campi Flegrei Caldera. *J Geophys Res Solid Earth* 1978 2012 110.  
611 <https://doi.org/10.1029/2004jb003102>
- 612 63. Vanorio, T., Kanitpanyacharoen, W., 2015. Rock physics of fibrous rocks akin to Roman con-  
613 crete explains uplifts at Campi Flegrei Caldera. *Science* 349, 617–621.  
614 <https://doi.org/10.1126/science.aab1292>
- 615 64. Waldhauser, F. 2001. HypoDD: A computer program to compute double-difference earthquake  
616 locations, USGS Open File Rep., 01-113.
- 617 65. Warren, N.W., Latham, G.V., 1970. An experimental study of thermally induced microfracturing  
618 and its relation to volcanic seismicity. *J. Geophys. Res.* 75, 4455–4464.  
619 <https://doi.org/10.1029/jb075i023p04455>
- 620 66. Wessel, P., Luis, J. F., Uieda, L., Scharroo, R., Wobbe, F., Smith, W. H. F., Tian, D., 2019. The  
621 Generic Mapping Tools version 6. *Geochemistry, Geophysics, Geosystems*, 20, 5556–  
622 5564. <https://doi.org/10.1029/2019GC008515>
- 623 67. White, R., McCausland, W., 2016. Volcano-tectonic earthquakes: A new tool for estimating in-  
624 trusive volumes and forecasting eruptions. *J. Volcanol. Geotherm. Res.* 309, 139–155.  
625 <https://doi.org/10.1016/j.jvolgeores.2015.10.020>
- 626 68. Wiemer, S., Wyss, M., 2000. Minimum Magnitude of Completeness in Earthquake Catalogs: Ex-  
627 amples from Alaska, the Western United States, and Japan. *B Seismol Soc Am* 90, 859–869.  
628 <https://doi.org/10.1785/0119990114>
- 629 69. Woo, J.Y.L., Kilburn, C.R.J., 2010. Intrusion and deformation at Campi Flegrei, southern Italy:  
630 Sills, dikes, and regional extension. *J Geophys Res Solid Earth* 1978 2012 115.  
631 <https://doi.org/10.1029/2009jb006913>

632

## 633 Captions

634

635

636

637

638

639

640

641

642

643

644

645

646

647

648

649

650

651

652

653

654

655

656

657

658

659

660

661

662

663

664

665

666

667

668

669

670

671

672

673

674

675

676

677

678

679

**Figure 1.** (A) Map of the Campi Flegrei area and geometry of the seismic monitoring networks in 1982-84 (squares managed by INGV-Naples (OV); circles managed by the University of Wisconsin), and after 2000 (triangles managed by INGV-Rome and upside-down triangles managed by INGV-Naples). Station STH is shown by the solid red triangle. The dotted gray line follows the inner edge of CFc (Natale et al., 2022). The dashed line offshore represents a segment of the inner edge of the caldera (Natale et al., 2022). 1=Monte Nuovo, 2=Astroni crater, 3=Pozzuoli, 4=La Starza marine terrace, S=Solfatara fumarole, P=Pisciarelli fumarole. (B) Vertical displacement at CFc from 1905 to December 2019 (De Martino et al., 2021). Red dots are levelling data at benchmark Bm25A, black dots are GPS measurements at Station RITE. Both sites (Bm25A and RITE) are in Pozzuoli (inset) (C) The gray bars are the number of VT seismic events per day for 1982-2023 (gray logarithmic scale). The green dots are the cumulative number of VT events per 6 months (logarithmic scale). The cyan dots are the cumulative seismic moment  $M_0$ , calculated with the method of Petrosino et al. (2008); secondary axes). The vertical displacement for 1982-2023 is referenced to 1905: red crosses are high-precision levelling measurements at benchmark Bm25A; red points are GPS measures at RITE station. (D) Map and vertical sections of the distribution of absolute (green) and relative (blue) seismic locations for the 1982-84 unrest. Vertical sections are cut along the two perpendicular transects AA' and BB' in map. (E) As for (D), but in 2005-23. The magnitudes of completeness are 0.5 for 1982-84 and 0.2 for 2005-23.

**Figure 2:** (A) Relative seismic locations for the 1982-84 time-window, in map (Panel 1) and vertical profile AB over time (Panels 2-5). Profile AB is oriented  $110^\circ\text{N}$ , 6 km long, and centred on Solfatara. The projected volume is 0.5 km wide. Circle size is proportional to magnitude (legend), colours change as a function of time (note the 1st Apr 1984 swarm in dark red); green circles indicate events with  $M \geq 3$ . The topographic elevation (in m) along the profile AB is plotted above the Panel 2 (elevations from Google Earth Pro). Pozzuoli, Astroni, Solfatara and Pisciarelli are marked in

659 cyan. The catalog has been truncated for a completeness magnitude  $M_c=0.5$ . (B) Map and vertical  
660 section for a perpendicular  $20^\circ\text{N}$ -oriented profile. Colours as for (A).

661 **Figure 3:** (A) Relative locations for the 1982-84 earthquakes in map (Panel 1) and vertical profile  
662 AB (Panels 2-5). Profile AB is NS-oriented, 6 km long, and centred on Solfatara. The projected  
663 volume is 0.5 km wide. Circle size is proportional to magnitude (legend), colours change as a func-  
664 tion of time (note the 1st Apr 1984 swarm in dark red); green circles indicate events with  $M \geq 3$ . The  
665 topographic elevation (in m) along the profile AB is plotted above the Panel 2 (elevations from  
666 Google Earth Pro). Pozzuoli, Astroni, Solfatara and Pisciarelli are marked in cyan. The catalog has  
667 been truncated for a completeness magnitude  $M_c=0.5$ . (B) Map and vertical section for a perpen-  
668 dicular EW-oriented profile. Colours as for (A).

669 **Figure 4:** (A) The relative locations for the 1<sup>st</sup> April 1984 swarm (red circles) superimposed on the  
670 background seismicity for the entire period 1982-84 (teal circles). The size of circles is proportional  
671 to the magnitude (legend in B). The green circles show the two  $M_d=3$  earthquakes. AB is the 6-km  
672 long profile,  $10^\circ\text{N}$ -oriented, used for the vertical section, and the box indicates the perimeter of the  
673 projected volume (1.5 km wide). (B) Vertical section along the profile AB (symbols as in (A)). The  
674 topographic elevation (in m, from Google Earth Pro) along the profile AB is plotted above the ver-  
675 tical section. (C) 3D representation of the swarm: absolute and relative locations are projected onto  
676 horizontal and vertical sections. The colour code changes with magnitude following the scale. The  
677 coast line is in black on the bottom plan. (D) Black points represent the daily measure of the ground  
678 displacement acquired by the tide gauge of Pozzuoli between 1982 and 1984 (primary axis; Berrino,  
679 1994). The blue dash-dotted line is the smoothed rate of uplift in cm per day (secondary axis).

680 **Figure 5:** (A) Relative locations of earthquakes with time for the 2005-23 in map (Panel 1) and ver-  
681 tical section AB (Panels 2-5). Profile AB is 60°N-oriented, 6 km long, and centred on Solfatara.  
2  
3  
682 The projected volume is 0.5 km wide. The size of circles is proportional to magnitude (legend).  
4  
5  
683 Colours change as a function of time (code on right). The green circles indicate events with  $M \geq 3$   
7  
684 during the 1982-84 unrest. The topographic elevation (in m) along the profile AB is plotted above  
8  
9  
685 Panel 2 (elevations from Google Earth Pro). Pozzuoli, Solfatara and Pisciarelli are marked in cyan.  
10  
11  
686 The catalog has been truncated for a completeness magnitude  $M_c=0.2$ . (B) Map and vertical section  
12  
13  
687 for a perpendicular 150°N-oriented profile, centred at Solfatara. Colours are the same code as in (A)  
14  
15  
688 **Figure 6:** Relative locations of VT events for 1982-84 (red circles) and 2005-23 (blue circles).  
16  
17  
689 Events of magnitude  $M \geq 3$  are shown by thick, dark circles. (A) Map of relative locations along six  
18  
19  
20  
690 8 km long profiles oriented at 40°N that cross CFC from SW to NE. Panels A-F show each vertical  
21  
22  
691 section. The projected volumes extend 0.25 km on each side of each profile. (B) Map and vertical  
23  
24  
692 section for the EW profile. The projected volume extends 0.5 km on each side of the profile. Col-  
25  
26  
693 ours as in (A).  
27  
28  
29  
30  
31  
694 **Figure 7:** Map and vertical sections of the Benioff strain for 1982-84 (red points) and 2005-2023  
32  
33  
695 (blue points). The black lines on the map are 6 km long profiles centred on Solfatara and radially  
34  
35  
696 spaced at 30°. The vertical sections give the square root of the seismic energy released in a 0.5 km  
36  
37  
697 wide volume projected onto each profile. Grey and green crosses in the EW oriented vertical section  
38  
39  
698 mark the D90 cutoff depth for the two distributions of seismicity 1982-84 and 2005-23, respectively.  
40  
41  
699 Pozzuoli, Solfatara and Pisciarelli are marked in yellow.  
42  
43  
44  
45  
46  
47  
48  
700 **Figure 8:** Maps of earthquake relative locations (green circles) of earthquakes for 1982-84 (A) and  
49  
50  
701 2005-2023 (B); red circles are events with  $M_d \geq 3$ . In both cases, XX' is the EW-oriented profile  
51  
52  
702 used for the vertical sections. The vertical sections represent the distribution of the Gutenberg-  
53  
54  
703 Richter  $b$ -value calculated in a volume 2 km wide around XX', the corresponding standard devia-  
55  
56  
704 tion  $\sigma_b$ , the magnitude of completeness  $M_c$  and the distribution of seismic locations projected on  
57  
58  
59  
60  
61  
62  
63  
64  
65

705 the vertical section. The topographic elevation along the profile XX' is obtained from Google Earth  
706 Pro. Pozzuoli, Solfatara and Pisciarelli are marked in yellow.

707 **Figure 9:** Variation of the  $b$ -value during 2005-2020 and 2021-2023. (A) Map of earthquake rela-  
708 tive locations (green and blue circles, code colour in legend) for the years 2005-2023. XX' is a EW-  
709 oriented profile used for the definition of vertical sections. (B) The vertical sections represent the  
710 distribution of the Gutenberg-Richter  $b$ -value for 2005-2020 ( $b_1$ ) calculated in a volume 2 km wide  
711 around XX' and the corresponding standard deviation  $\sigma_{b_1}$ . The topographic elevation along the pro-  
712 file XX' is obtained from Google Earth Pro. (C) As for B for 2021-2023 ( $b_2$ ). (D) The difference  
713  $\Delta b = b_2 - b_1$  and corresponding standard deviation  $\sigma_{\Delta b}$ . The distribution of seismicity in 2005-2023  
714 (blue points) is superimposed on  $\Delta b$ . Pozzuoli, Solfatara and Pisciarelli are marked in yellow.

715 **Fig. 10:** Conceptual model of unrest at CFc since 1982. (Top) The sequence of ground vertical de-  
716 formation in 1982-84, 1985-2005 and 2005-2021 obtained from levelling measurements at bench-  
717 mark Bm25A (Pozzuoli) and at the cGPS station RITE (De Martino et al., 2021). (Middle) The cor-  
718 responding relative locations of earthquakes (blue). Events with  $M_d \geq 3$  are shown in red. (Bottom)  
719 Vertical sections with relocated seismicity projected along the EW profile (AA') and cartoon of the  
720 state of fracturing across the BDTZ as suggested by seismicity.

Graphical Abstract (for review) **reaching** Brittle hydrothermal  
**Campi Flegrei** swarm: **Seismicity** ductile fluids  
 injection depressurization Pisciarrelli **unrest** fracture uplift fluids  
 caldera magma scenario—pressurization Pozzuoli fumarole stress

# EVOLUTION IN UNREST PROCESSES AT CAMPI FLEGREI

## CALDERA AS INFERRED FROM LOCAL SEISMICITY

S. Danesi, N.A. Pino, S. Carlino and C.R.J. Kilburn, *EPSL* 2023

### CONCLUSIONS

Low permeability structural barriers modulate fluid circulation which in turn favours seismicity.

Recent fluid circulation increases crack density and reduces host rock resistance, shifting *b*-values to high values (higher than in 1982–84 and increasing recently).

The deactivation of the unrest may follow the break of the brittle/ductile transition.

Uplift is likely to continue until weakening of the brittle/ductile transition and crustal fracturing allow the source to be depressurised.

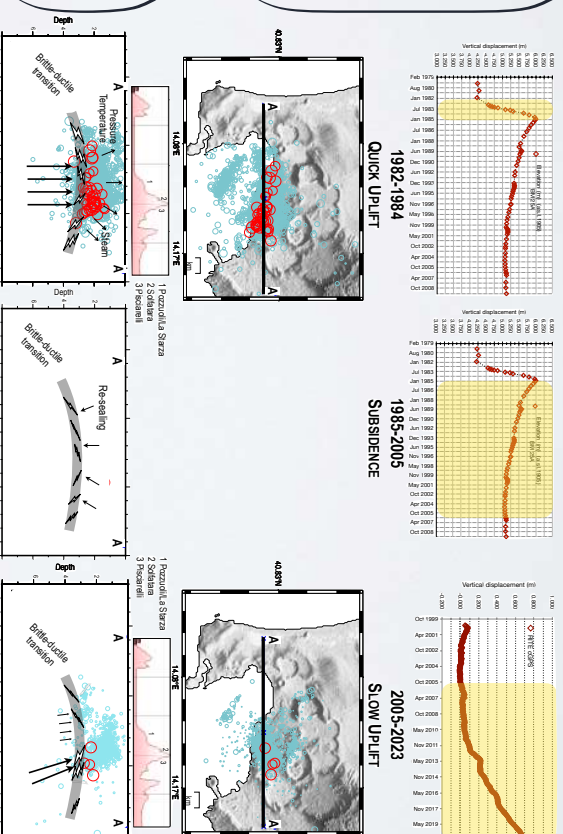
### WHY

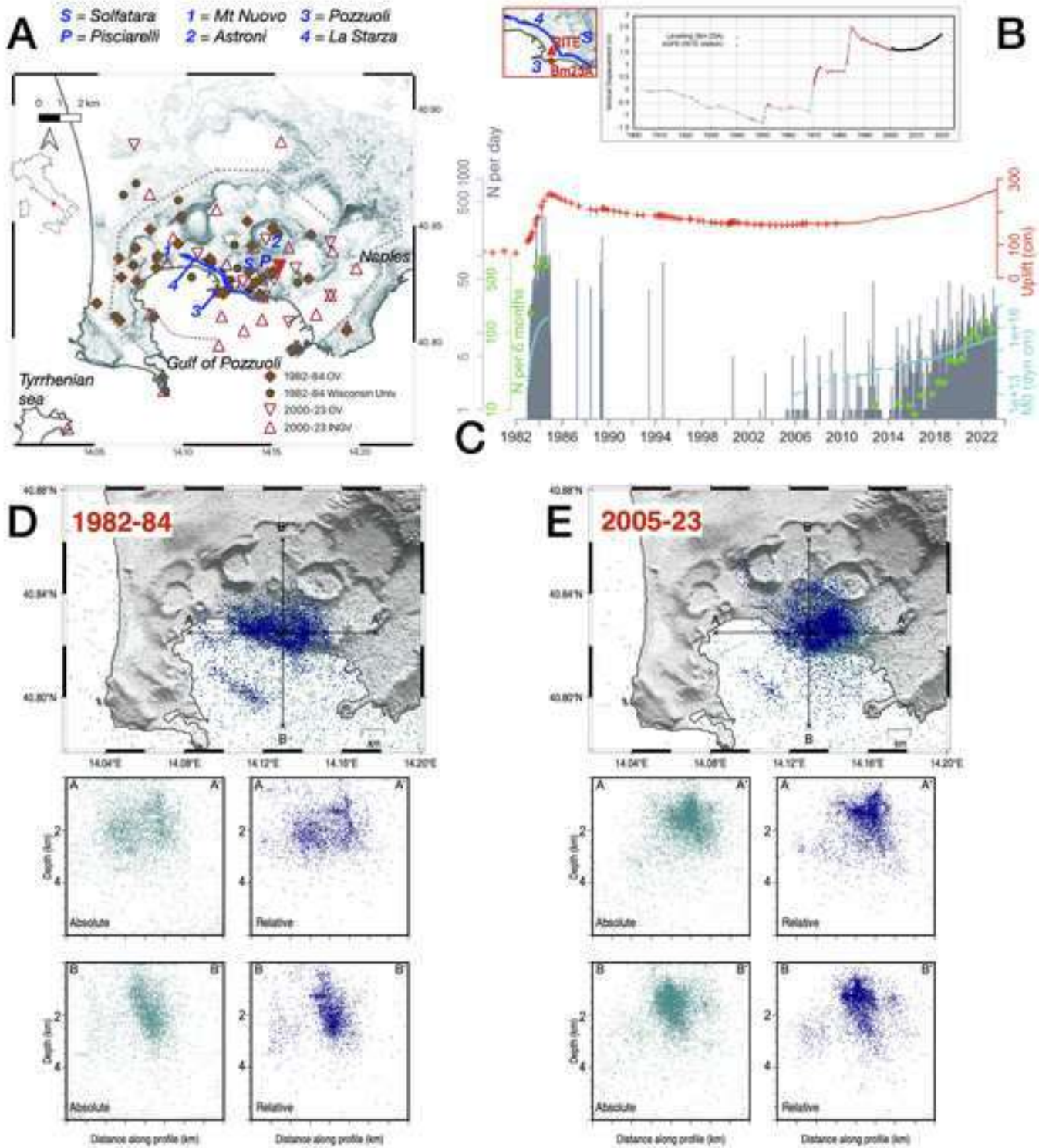
The current uplift (2005–2023) exceeds the deformation observed in any previous period of unrest, since instrumental monitoring began. An escalation in seismicity has been observed, with increasing rate since 2018.

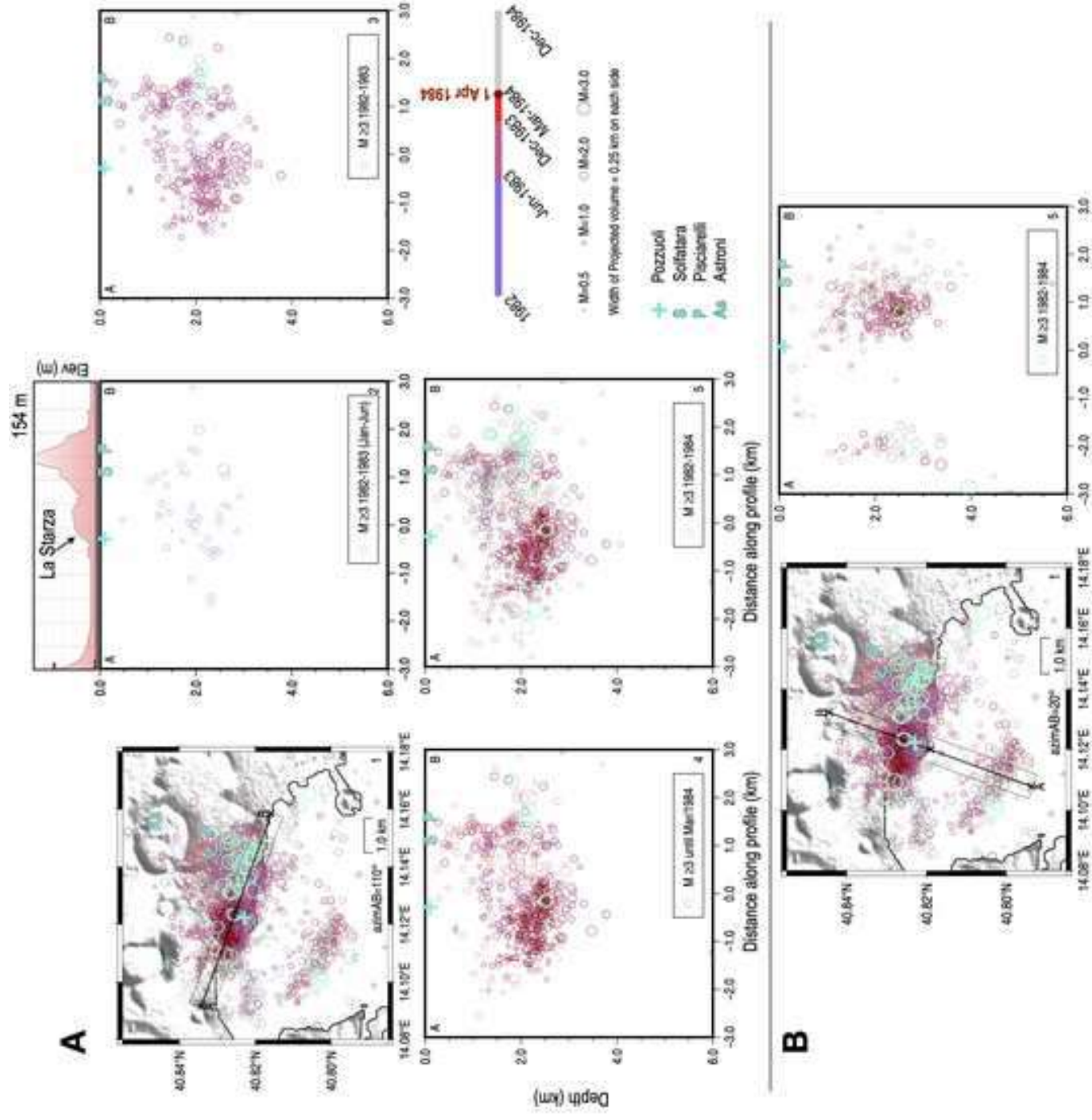
Unlike in 1982–84, the seismicity is asymmetric with respect to the point where the maximum uplift is observed.

### HOW

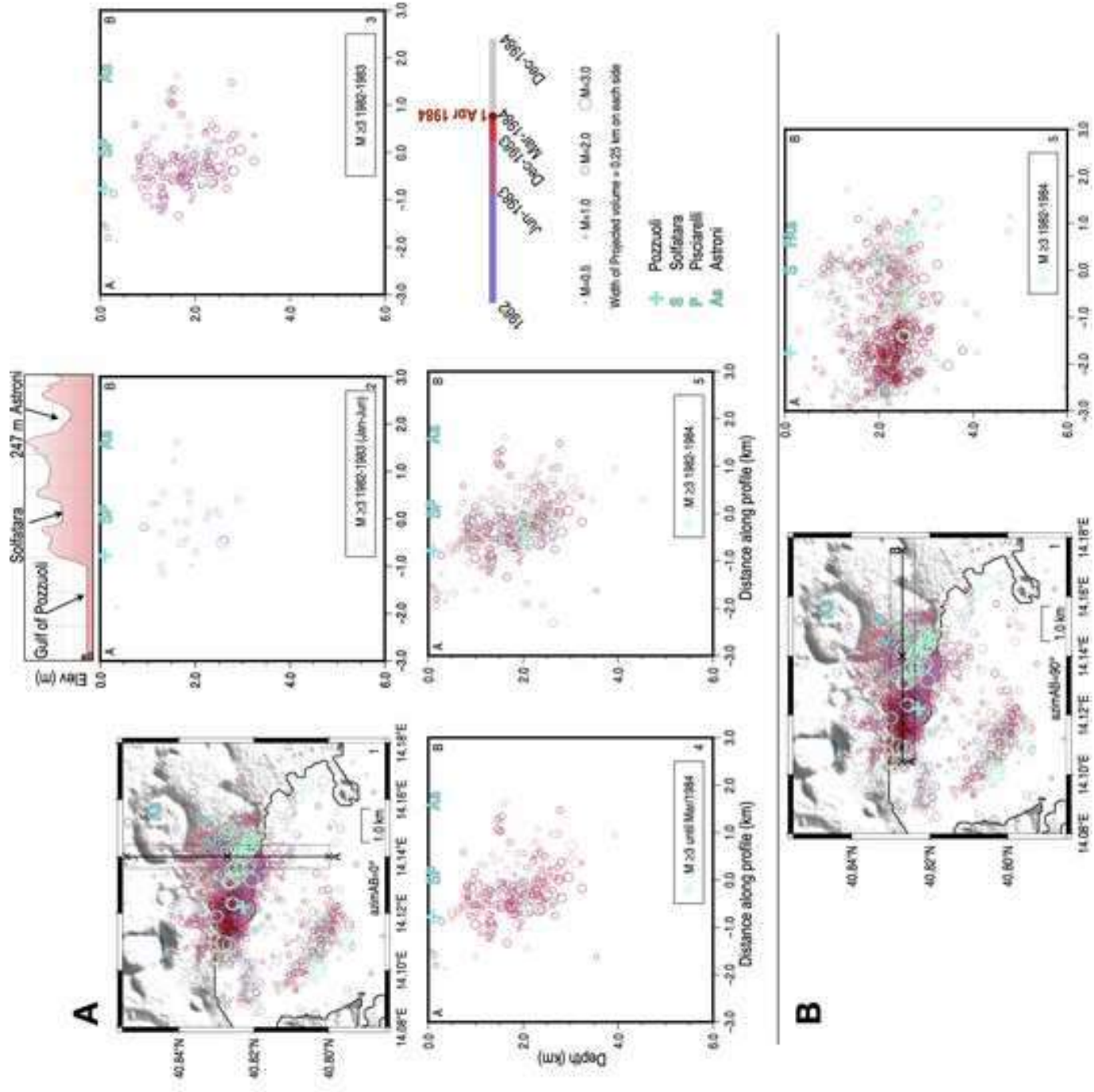
Space and time evolution of the volcano-tectonic seismicity; cumulative seismic energy calculated from the Benioff strain and Gutenberg-Richter *b*-value.

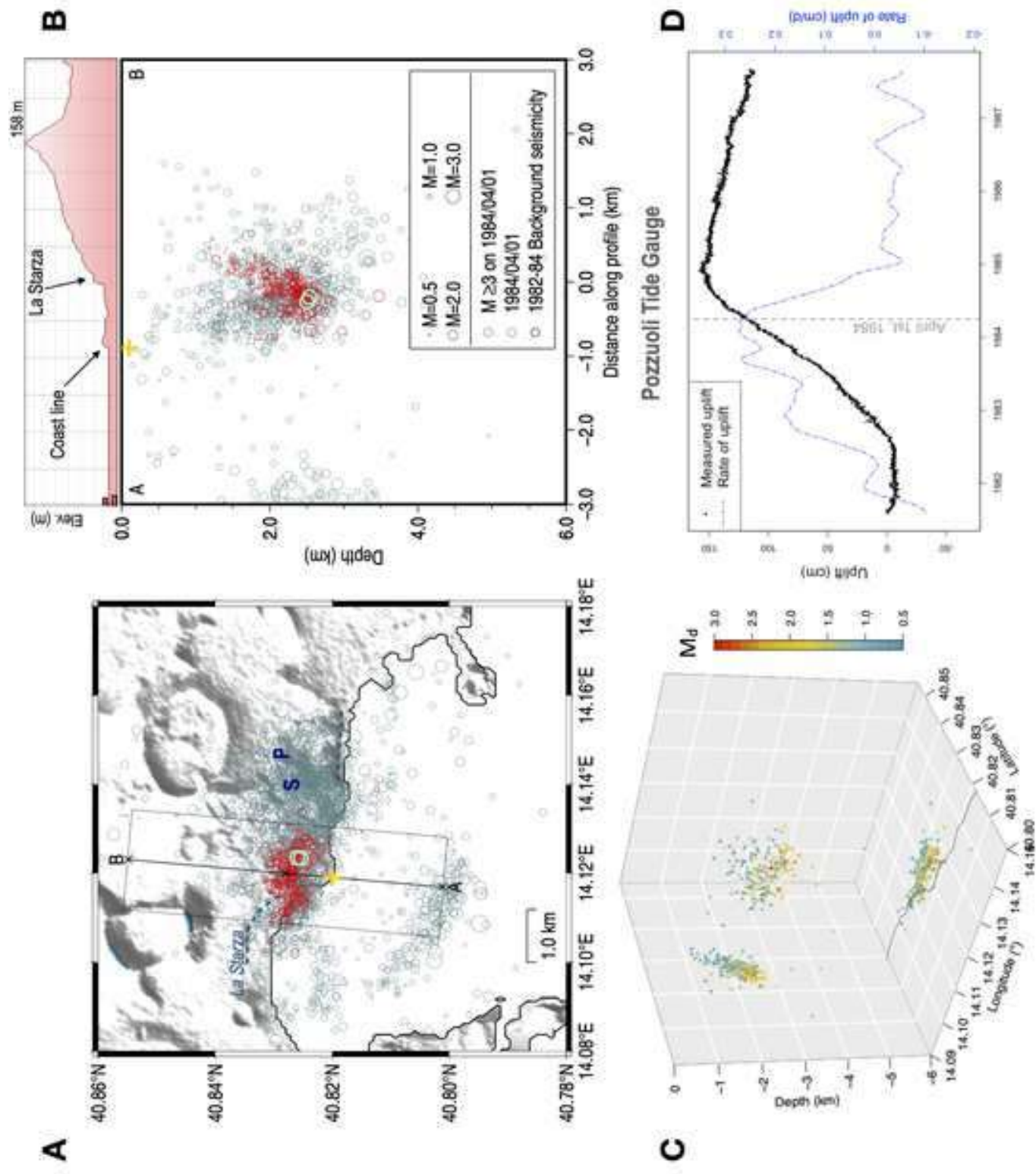


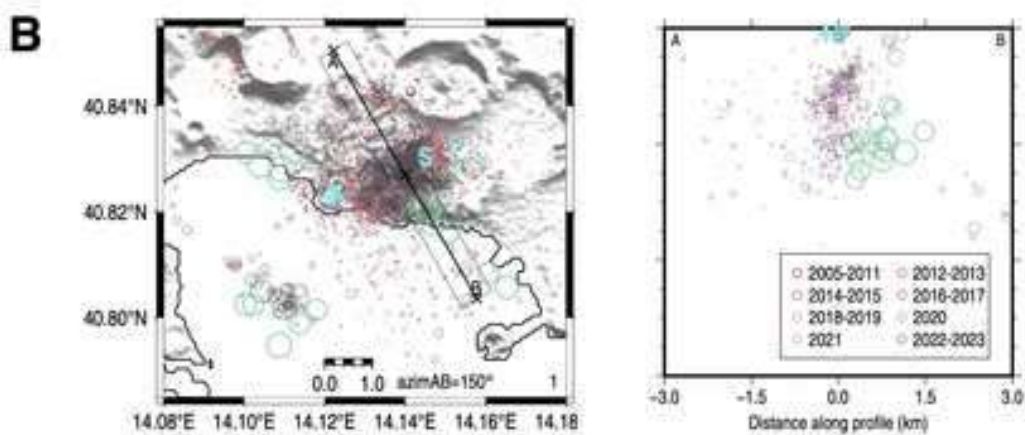
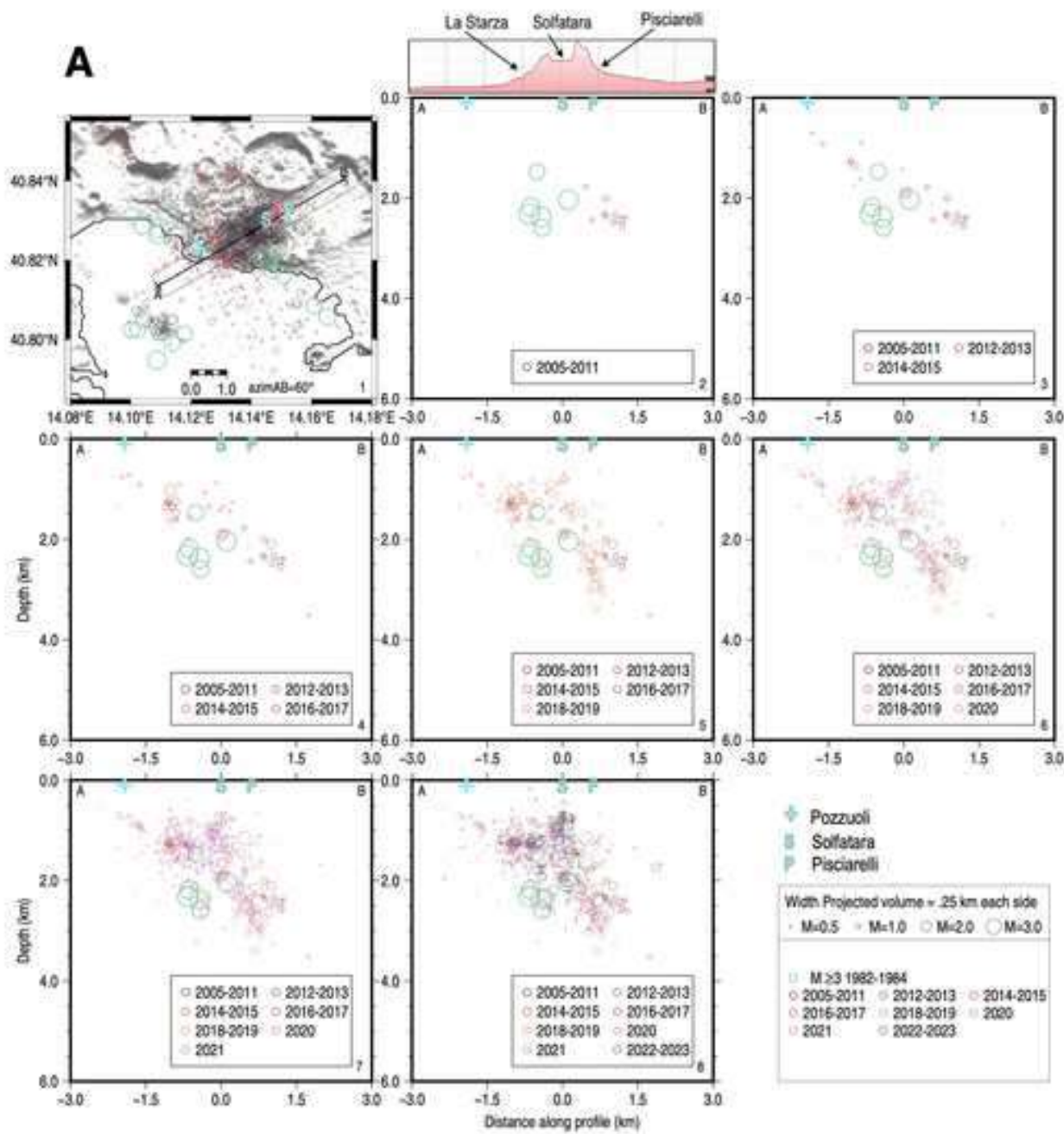


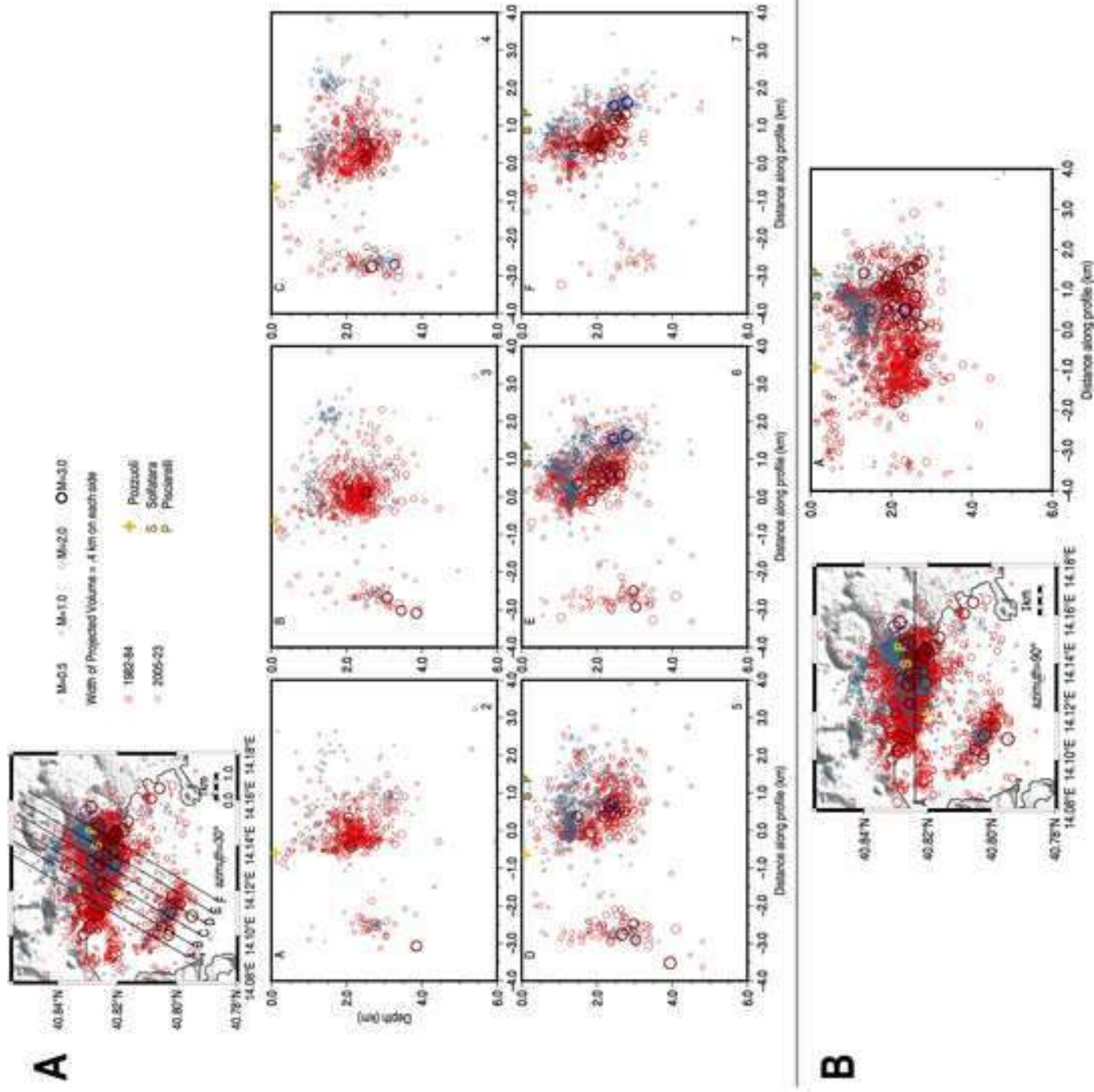


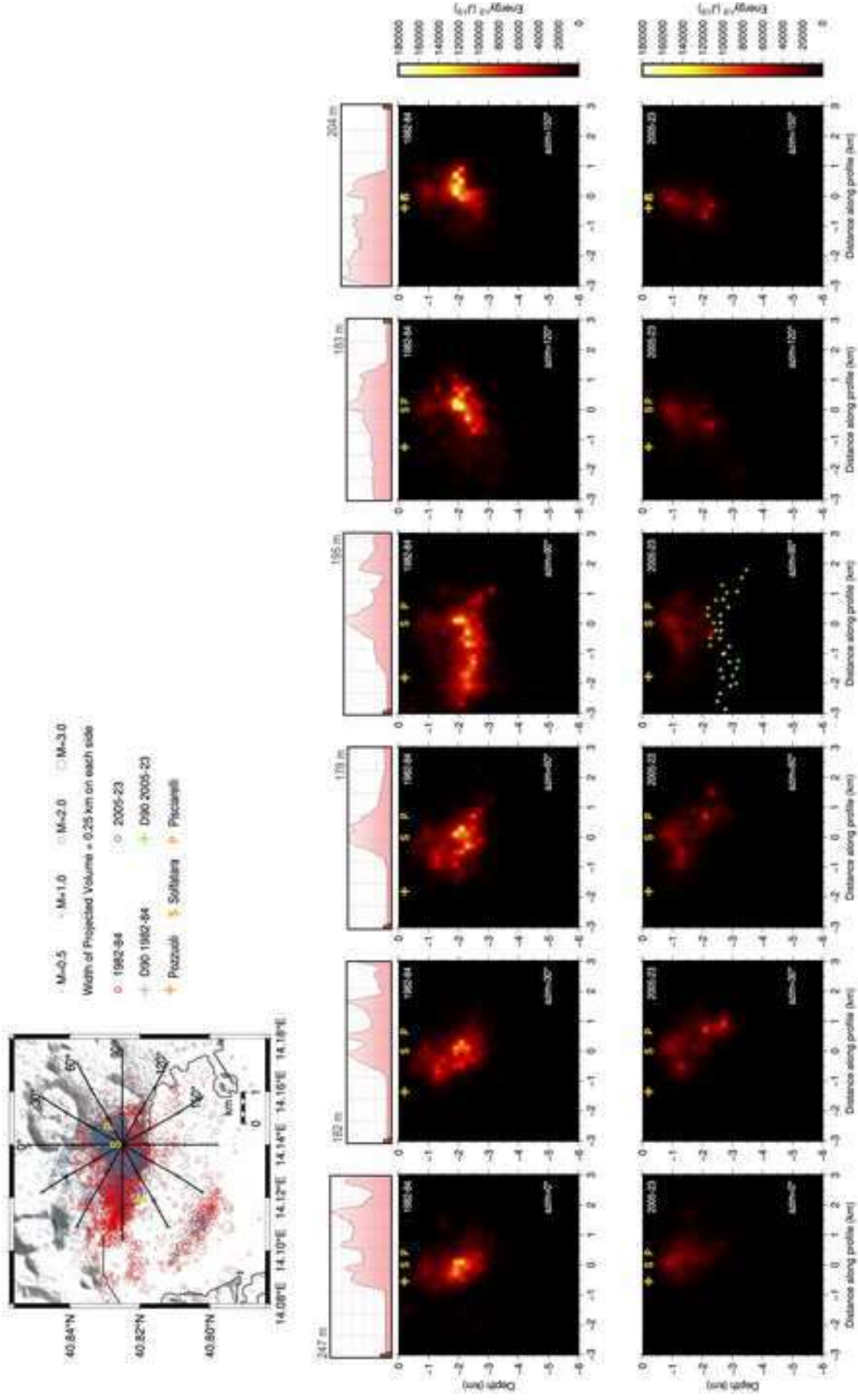


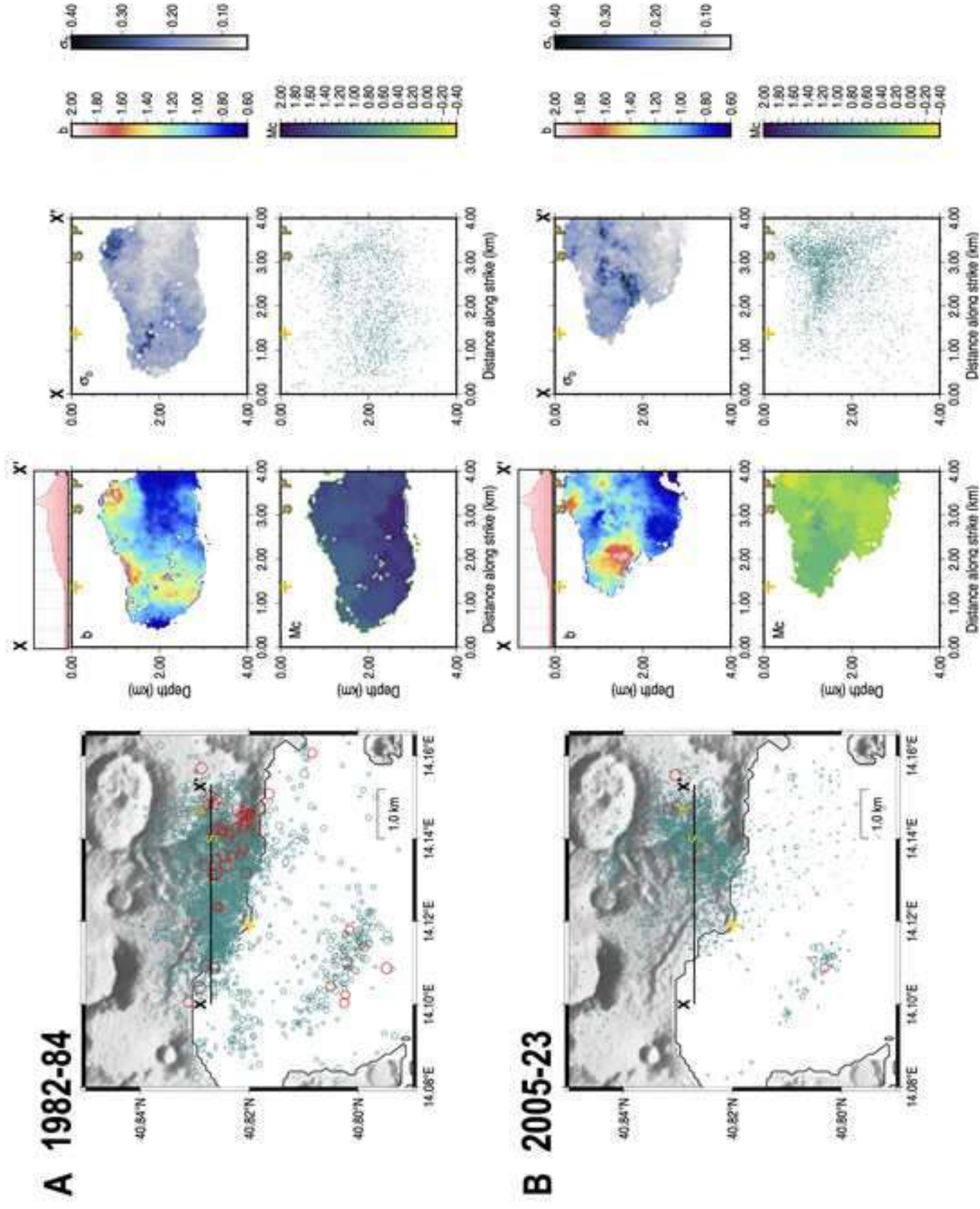


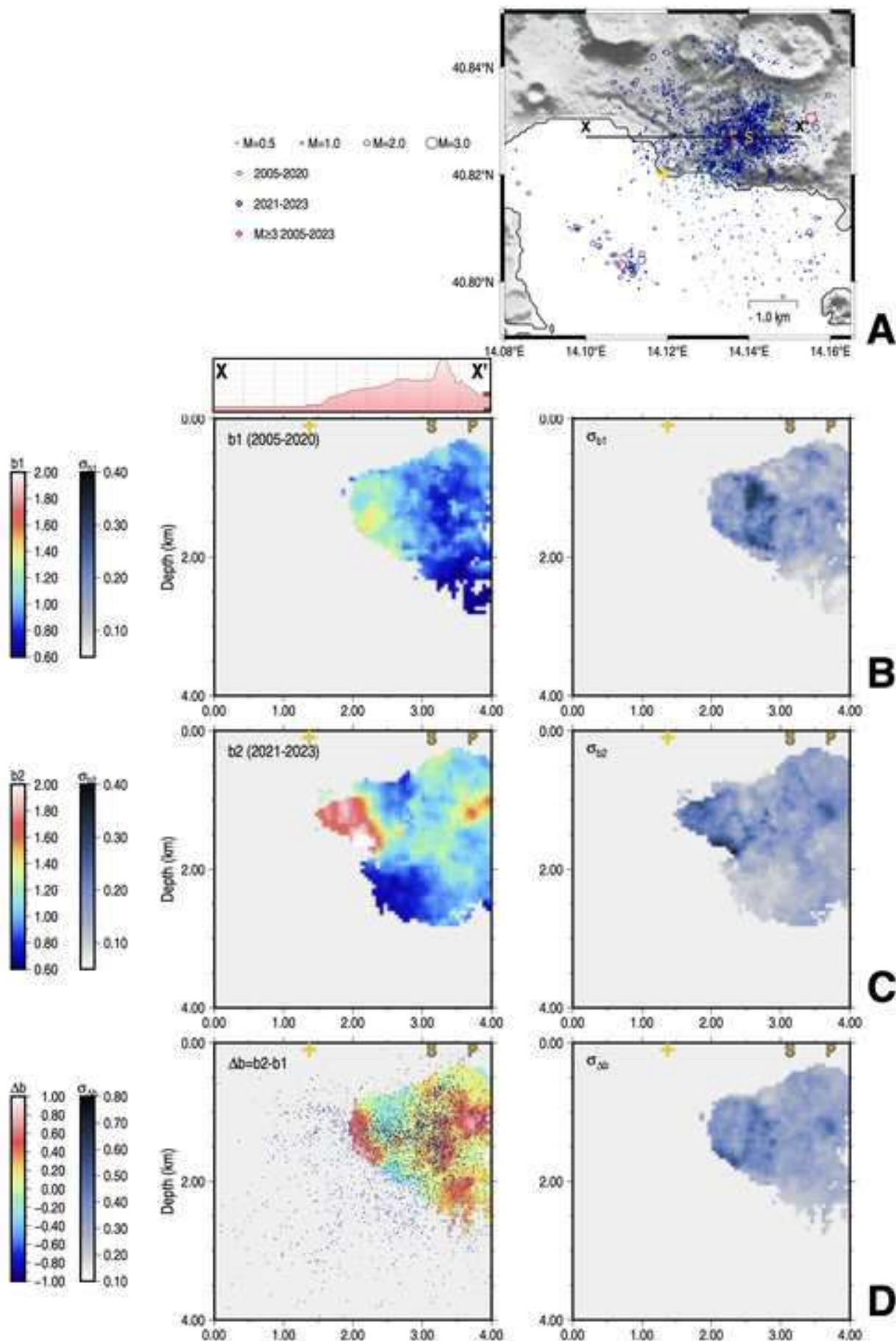


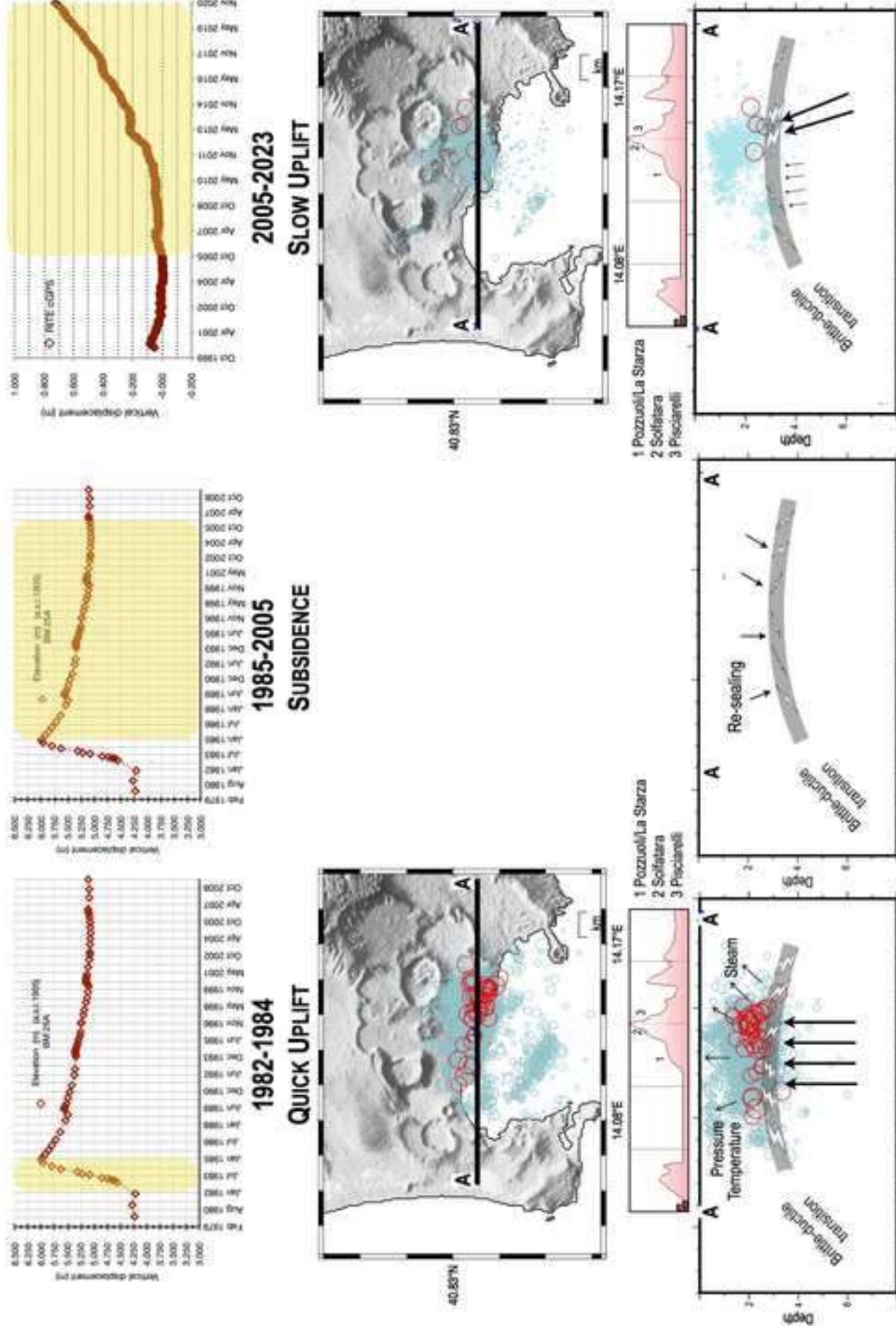














Figure\_1 (high-resolution)



Click here to access/download  
**Figure (high-resolution)**  
Figure\_1.pdf

Figure\_2 (high-resolution)



Click here to access/download  
**Figure (high-resolution)**  
Figure\_2.pdf



Figure\_3 (high-resolution)



Click here to access/download  
**Figure (high-resolution)**  
Figure\_3.pdf



Figure\_4 (high-resolution)



Figure\_5 (high-resolution)



Click here to access/download  
**Figure (high-resolution)**  
Figure\_5.pdf



Figure\_6 (high-resolution)



Figure\_7 (high-resolution)



Figure\_8 (high-resolution)



Click here to access/download  
**Figure (high-resolution)**  
Figure\_8.pdf





Figure\_9 (high-resolution)



Click here to access/download  
**Figure (high-resolution)**  
Figure\_9.pdf



Figure\_10 (high-resolution)



Supplementary material for online publication only



[Click here to access/download](#)

**Supplementary material for online publication only**  
**Supplementary.pdf**

